Wesleyan University The Honors College

Hα Dots : The Nature of Isolated Extragalactic Emission Line Sources

by

Jessica Kellar

Class of 2008

A thesis submitted to the
faculty of Wesleyan University
in partial fulfillment of the requirements for the
Degree of Bachelor of Arts
with Departmental Honors in Astronomy

Middletown, Connecticut April, 2008

Acknowledgements

I would like to thank my advisor, John Salzer, for being an inspirational mentor. I have learned so much from doing research with you and I feel really lucky to have had this opportunity. Thank you for spending so much time working with me and for listening to all my crazy ideas. Thank you for always being so encouraging and supportive. Thank you for inspiring my love of astronomy. (And thank you also for not pushing me off the cliff at MDM, yet...)

I would like to thank Gary Wegner for the opportunity to take spectra of the Hα dots at MDM. Without the opportunity to take these follow-up spectra we would never have known what the Hα dots are. Thank you for having confidence in my ideas and for all our telescope conversations. I would like to thank Roy Kilgard for always being so willing to answer my questions and discuss ideas with me. I've really appreciated that your door is always open and thanks for all the advise you have given me. To Ed Moran, thank you for always being so encouraging and for giving me lots of advice about my research. To Kathryn Johnston, thank you for giving me my first opportunity to go observing and do astronomy research; and thank you for encouraging me to be an astronomy major.

I would like to thank my fellow astronomy majors and in particular the other thesis writers. Evan and Arthur - those long nights in the observatory "dungeon" would have been a lot less fun without you guys. I would like to acknowledge all the students who have read and given insightful comments on various portions of this thesis - Karlin, Elissa, Sam, Darik, and Danielle.

I would like to thank my friends for keeping me sane (or in some cases making me more insane...) Thank you to the San Francisco Side Walk Astronomers for

bringing out your telescopes on those rare clear nights in the city and encouraging little kids to look up at the stars. Thank you to my cat, dog, mom, dad, and brother for being so supportive and always encouraging me to follow my passions.

Contents

Chapter 1

Introduction

To see a world in a grain of sand,

And a heaven in a wild flower,

Hold infinity in the palm of your hand,

And eternity in an hour.

- William Blake, Auguries of Innocence

1.1 The Quest to Understand Our Universe

What happens in the space between the galaxies? How do galaxies form and what causes star formation? How can we even begin to answer such large questions from as insignificant of a spot in the universe as planet earth?

Since the beginning of human history people have looked to the stars and asked questions. Ancient peoples associated the patterns of stars they saw in the sky with mythological stories. As technology improved, our ability to probe the universe and gain insight into fundamental questions has increased. The advent of the telescope allowed astronomers to probe distances that had previously been in-

accessible to the human eye. And later, the development of the photographic plate and modern CCD detectors revolutionized astronomy by allowing astronomers to record the light they collected and perform precise measurements.

As technology expanded, so did our view of the universe. Initially, it was thought that Earth was the center of the universe. Copernicus and Galileo proved that in fact Earth revolved around the Sun. Eventually, the existence of other stars was determined; however, it was still believed that our galaxy was an "island universe". It was not until Hershel's observations of the spiral nebulae that we even had an inkling that our galaxy, the Milky Way, might in fact be just one galaxy in a universe filled with many galaxies.

In modern times, with space-based telescopes, adaptive optics, and very sensitive equipment we can study galaxies at far reaching distances and in greater detail than ever before. Yet, fundamental questions about galaxy formation and evolution still remain unanswered. In some sense, the more we learn about the universe, the more we realize we don't know.

A key issue in understanding galaxy formation and evolution is star formation. Galaxies are composed of gas, dust, and stars. It is the stars in galaxies that emit light that we can observe and allow us to study them. In particular, the formation of stars gives insight into the evolution of galaxies. As stars form and die the chemical composition of the gas and dust in the galaxy is affected. Galaxies in which star formation occurs differ dramatically from those in which it does not. How common star formation is in our universe and where it occurs remain pressing questions.

1.2 Galaxies and Star Formation

Many surveys have been done to study star formation, both in our local universe and over large ranges of distances. In order to know where to look to study star formation, it is useful to consider the environmental factors that are necessary for star formation to occur. As was first shown by Cecilia Payne-Gaposchkin in her 1925 Ph.d thesis on stellar atmospheres, stars are predominantly composed of hydrogen (Payne-Gaposchkin 1925). Thus the environment in which star formation occurs must contain hydrogen. This is not to say that all regions of the universe that contain hydrogen are forming stars. There is a certain critical density of hydrogen that is necessary for star formation to begin.

We do not have a complete understanding of how protostars form from molecular hydrogen gas. The condition of equilibrium for a stable, gravitationally bound gas cloud is described by the virial theorem:

$$2K + U = 0. \tag{1.1}$$

The idea is that once a certain density is reached and the potential energy (U) of the gas dominates over its kinetic energy (K), the molecular hydrogen cloud will become gravitationally unstable and will begin to collapse. There is a minimum mass, known as the Jeans mass, that is necessary for spontaneous collapse of the cloud to occur. Rather than a single massive star forming from this gravitational collapse, typically the collapsing cloud will fragment so that multiple stars form (Carroll and Ostlie 2007).

There are many ways in which star formation can be studied using different wavelength ranges which cover different portions of the electromagnetic spectrum - Infared, Ultraviolet, X-ray, Radio, Optical. Light emitted by young stars in

star-forming regions is often absorbed by dust and re-radiated in the far infared. Ultraviolet can be used to directly study the photons emitted by hot O and B type stars. High mass X-ray binaries indicate populations of young stars. Radio wavelengths can be used to study neutral hydrogen, which indicates an environment in which star formation could potentially occur. Optical observations can be used to study the star formation rate from young O and B stars.

1.2.1 Neutral Hydrogen

Neutral hydrogen (HI) can be studied by observing the 21 cm radio emission line. Electrons and protons have spin quantum numbers. There are two possible orientations for the spin vectors: up and down. The energy of the atom varies depending on the spin configuration of the proton and electron. If the spins of the electron and the proton are aligned (both spin up or both spin down) the atom has slightly more energy than if the electron and proton are anti-aligned (one spin-up and one spin-down). If the spin of the electron flips from being aligned with the proton to being anti-aligned with the proton a discrete amount of energy is emitted. A 21 cm photon is emitted only if the spin flip transition occurs in a hydrogen atom in isolation, not as the result of the collision between two hydrogen atoms. Therefore the 21 cm line can be used only to study hydrogen in very low density regions. It takes a long time (several million years) before an electron in an isolated hydrogen atom makes a spin flip transition (Carroll and Ostlie 2007). However because there are so many neutral hydrogen atoms in the interstellar medium of galaxies this still amounts to a large amount of radiation. Since the intergalactic medium is very low density, this transition will eventually occur. By detecting 21 cm emission we can study the distribution of HI in the

universe. Since hydrogen is the most abundant element in the universe, studying its distribution has many applications in astronomy. One important application is using the distribution of neutral hydrogen to indicate environments in which star formation could potentially occur.

1.2.2 Hα Emission and HII regions

When star formation occurs, young hot O and B spectral type stars emit photons with energies greater than 13.6 eV (in the ultraviolet portion of the spectrum). These photons have enough energy to ionize the surrounding ground-state neutral hydrogen gas. This ionization results in free electrons and protons. The free electrons and protons will recombine to form neutral hydrogen atoms. The energy levels in an atom are quantized. So when an electron makes a transition between two different energy levels, a discrete amount of energy is released. After recombining with a proton, an electron will not necessarily fall immediately from infinity to the ground state. There are different probabilities that different transitions will occur (Griffiths 2005). Each transition corresponds to a different amount of emitted energy that corresponds to a specific wavelength. The transition between the n=3 and n=2 energy levels releases a photon that corresponds to a wavelength of 6563 Å which is easily observable within the optical wavelength range. This is known as Hα emission. By detecting Hα emission, we can infer regions of ionized hydrogen (HII regions). These regions of ionized hydrogen indicate that star formation is taking place. One important assumption that is made is that the rate of ionization is equal to the rate of recombination. This is not necessarily true, especially right in the beginning of the star formation process. However, eventually as the ionized gas expands, it reaches a state of equilibrium

in which these two rates are equal. Based on this assumption, the amount of star formation in a galaxy can be calculated based on the amount of Hα emission that is observed.

1.3 The ALFALFA Survey and the ALFALFA Hα Survey

The Arecibo Legacy Fast ALFA (ALFALFA) survey is an HI survey currently taking place at Arecibo with a goal of observing about 7000 square degrees of the sky (Giovanelli et al. 2005). ALFA is the Arecibo L-band feed array. The survey will cover a redshift range between -1600 and 18,000 km/s with about 5 km/s resolution. The goals of the survey include probing the faint end of the HI mass function, providing a census of HI to faint flux limits, and searching for HI tidal features. ALFALFA will not be biased towards high surface brightness galaxies usually found in optical galaxy catalogs.

The ALFALFA Hα survey (Sugden 2008) is a follow-up optical survey to study the star-formation rate in the local universe. It is a volume-limited survey so it does not suffer strongly from sample selection biases, such as the Malmquist bias, that affects magnitude-limited surveys. The Malmquist bias results in a disproportionally large number of luminous galaxies detected since luminous galaxies are easier to detect than lower-luminosity ones. Therefore magnitude-limited surveys end up with a biased representation of the population of galaxies since many more luminous galaxies will be found than dwarf galaxies. When studying a phenomenon such as star formation it is important to survey both luminous and dwarf galaxies since the attributes of galaxies of different luminosities may be very

different. By taking follow-up optical observations of a volume-limited sample of galaxies selected from the ALFALFA survey, the population of galaxies observed will be representative of the true distribution of potential star-forming galaxies in the local universe. Moreover, a statistically complete determination of the star-formation rate in the local universe can be obtained.

In order to conduct the ALFALFA Hα survey, optical observations of each target galaxy are taken using a continuum R and narrow-band Hα filter with the Kitt Peak National Observatory (KPNO) 0.9 meter telescope. During the image reduction process, a scaled version of the R image is subtracted from the Hα image in order to determine the Hα flux in the target galaxy and thus derive a star-formation rate. The amount of star formation varies drastically from galaxy to galaxy; some galaxies have large amounts of star formation, some have small amounts, and others have none. The field of view that was used on the S2KB CCD detector of the 0.9 meter telescope was 15 by 15 arcminutes. Typically the target galaxy is centered in the middle of the image and each image covers a much larger portion of the sky than just the target galaxy. The expectation is that by subtracting the R image from the Hα image, all the other objects would disappear and the resulting continuum-subtracted Hα image would contain only Hα flux from the target galaxy. From this Hα flux we would be able to determine the star-formation rate of the target galaxy.

1.4 Unexpected Dots

While reducing one of the fields, agc002134, we noticed something unusual in the data. The agc002134 target galaxy is the spiral in the center of Figure 1.1 (continuum R image) and Figure 1.2 (continuum-subtracted Hα image). The target

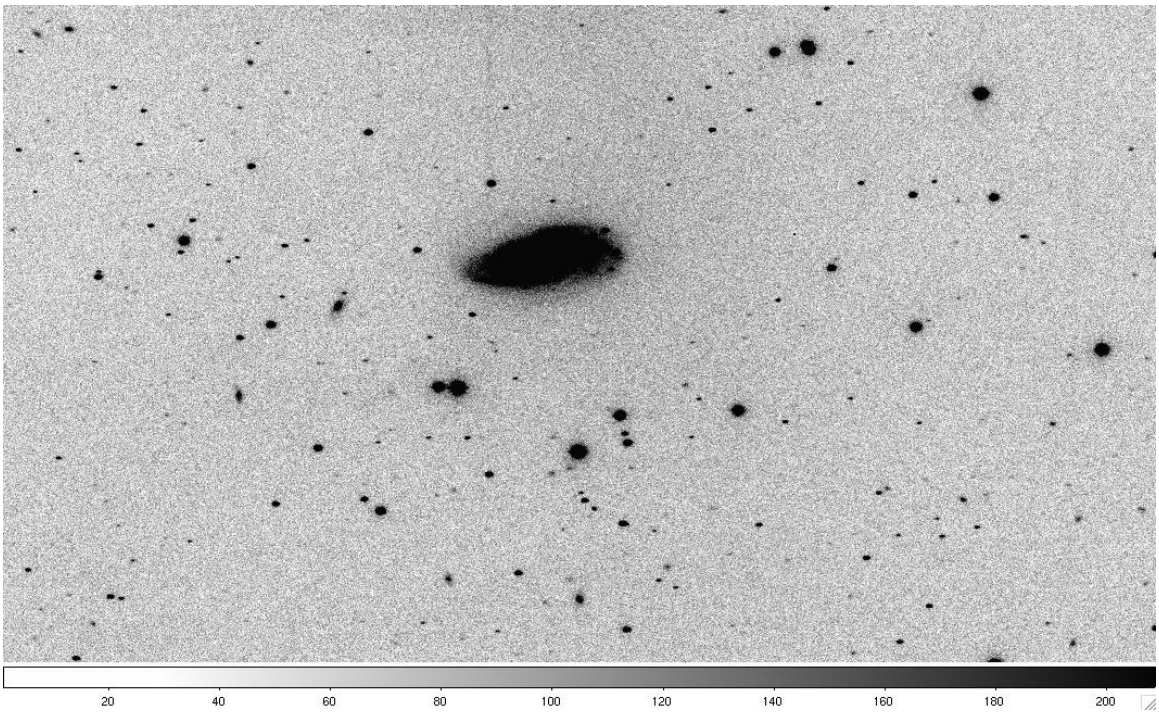

Figure 1.1: Continuum R image of the field centered around the target galaxy agc002134. The target galaxy is the spiral in the center of the image.

spiral in the center of Figure 1.2 clearly has Hα emission in its nucleus and along its spiral arms. In Figure 1.1 the target spiral is surrounded by many other objects. Most of these objects disappear completely in Figure 1.2 since the R flux of the objects is equal to the Hα flux of the objects so the subtraction results in the removal of the objects in the resultant Hα continuum-subtracted image. The subtraction is not perfect and for bright stars residual marks are often left in the subtracted image. In Figure 1.2 some instances of imperfect subtraction can be seen scattered throughout the image as partially subtracted stars. Partially subtracted stars can be identified based on their appearance since some of the pixels in the object have been over-subtracted and some under-subtracted. We emphasize that real detections of Hα can be distinguished from partial subtractions of saturated stars based on visual appearance.

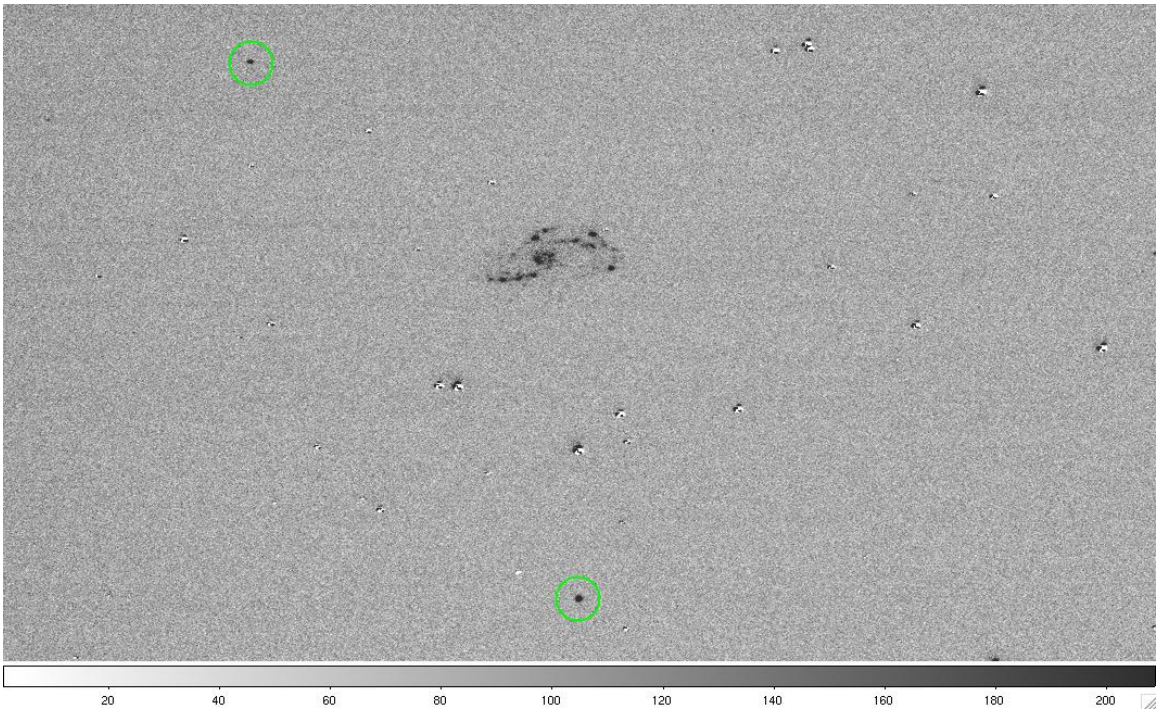

Figure 1.2: Hα continuum-subtracted image of the same field shown in the previous figure, centered around the target galaxy agc002134. Note the two distinct dots of Hα emission that are clearly separate from the spiral galaxy in the center, and not associated with the bright stars seen in the continuum image. One dot is in the upper left of the image and the other is in the bottom, almost directly below the spiral galaxy in the image. This is the first image in which two Hα dots were originally and unexpectedly noticed by eye during the image reduction process.

When we looked at the Hα continuum-subtracted image in Figure 1.2 there appeared to be two distinct dots of Hα emission that were separate from the target galaxy. Each of these dots of Hα emission correspond to an object in the R band continuum image in Figure 1.1. This seemed strange since the expectation was that by subtracting the R image from the Hα image only the Hα flux in the target galaxy would remain in the Hα continuum-subtracted image. Initially we assumed that these two dots of Hα emission separate from the target galaxy must have been caused by a mistake in the image reduction. So all the image reduction steps were thoroughly rechecked. After rechecking the image reduction steps, it seemed as though no image reduction mistake had been made and the two dots of Hα were, in fact, indications of isolated Hα emission.

Our unexpected observation of the two dots of Hα emission (hereafter referred to as Hα dots) led to a series of questions. What are these Hα dots? Do they exist in other images? How common are they? Are they associated with the target galaxy in the field or are they independent regions? Could they be background objects that are at a greater distance than the target galaxy? Are they small isolated regions of star formation? What would cause star formation to occur so far outside normal galaxies?

The primary motivation for this thesis is our desire to answer these questions. The goals of this thesis are to detect, catalog, and understand the nature of Hα dots.

1.5 Other Emission-Line Surveys

The significant emission in the Hα dots is indicative of some type of activity in the dot. It is likely that the Hα dots are emission-line galaxies. There are two main

types of emission-line galaxies: Active Galactic Nuclei (AGN) and star-forming galaxies. They are distinguished based on the dominant source of emission. In AGNs, the dominant source of activity is the accretion of material onto a black hole. In star-forming galaxies the dominant source of activity is caused by ultraviolet photons emitted by hot O and B type stars. Emission-line galaxies are thought to compose 5 to 10 percent of the total number of galaxies in the universe (Salzer 1989; Gregory et al. 2000). Many surveys have been done to study emission-line galaxies. Three emission-line surveys - KPNO International Spectroscopic Survey (Salzer et al. 2000), Survey for Low-Luminosity Emission-line Galaxies (Boroson, Salzer, and Trotter 1993), and Intergalactic HII regions Discovered in SINGG (Ryan-Weber et al. 2003; Werk et al. in preparation) - were particularly influential in the development of this thesis.

1.5.1 KISS

The KPNO International Spectroscopic Survey (KISS) combines the advantages of an objective prism and modern CCD detector to search for emission-line galaxies (Salzer et al. 2000). As a result of the use of a CCD, it reaches fainter flux limits than previous photographic surveys for emission-line objects. It covers roughly 200 square degrees of the sky and has detected more than 2500 objects. The goals of the survey are to create a sample of objects that can be used to gain insight into questions about galaxy formation and evolution, chemical evolution, large-scale structure, and cosmology. The Hα dot survey also seeks to answer questions about galaxy formation, evolution and chemical composition. Although the Hα dot survey uses narrowband photometry rather than an objective prism to identify emission-line candidates, many of the techniques and software that are

used to identify KISS galaxies served as a reference when developing the selection method and creating the software to detect Hα dot candidates.

1.5.2 Survey for Low-Luminosity Emission-Line Galaxies

The Survey for Low-Luminosity Emission-Line Galaxies (hereafter referred to as the Boroson survey) uses five narrow-band filters to detect emission-line objects (Boroson, Salzer, and Trotter 1993). It covers 0.7 square degrees of the sky. Using five narrowband filters is advantageous, since objects in which most of the flux is in a narrow emission line would appear much brighter through one of the filters than through the others. The survey detects objects with strong emission lines such as Hα, [O III]λ5007 and [O II]. The goals of the survey include finding candidate emission-line galaxies of very low luminosity, using this sample to calculate the faint end of the luminosity function, and detecting ultra-low metal-abundance galaxies. The benefit of selecting objects based on the strengths of their emission lines is that objects with faint continuum-emission and strong emission lines, which would otherwise be missed, can be found. The survey consists of identifying emission-line candidates and obtaining follow-up spectra to determine whether or not the objects are in fact emission-line objects. About 300 emission-line candidates were selected based on a (line+continuum)/continuum ratio criteria. The results of the follow-up spectra indicate that eleven low redshift objects (z less than 0.054) were detected by Hα and 36 emission-line galaxies at higher redshifts were detected by other strong emission lines such as [O III]λ5007 and [OII]. Like the Boroson survey, the Hα dot survey is also a narrow-band emission-line survey and is sensitive to low-luminosity objects that have strong emission lines. The selection method used to detect Hα dot candidates is in large part based on the

selection method used to detect emission-line galaxies in the Boroson survey.

1.5.3 Intergalactic HII Regions discovered in SINGG

Of the surveys mentioned above, the Intergalactic HII Regions discovered in SINGG (Ryan-Webber et al. 2003; Werk et al. in preparation) most closely connects to the work presented within this thesis. A number of small HII regions have been discovered that are clearly separate from the nearest galaxy in the field. These isolated HII regions were found in the narrowband Hα images obtained by the NOAO Survey for Ionization and Neutral Gas Galaxies (SINGG). SINGG is an optical Hα follow-up survey of an HI selected sample of galaxies from the HI Parkes All-Sky Survey (HIPASS; Barnes et al. 2001; Meyer et al. 2003). The isolated HII regions found in the SINGG survey are at projected distances of up to 30 kpc from their nearest galaxy. Based on the large separation between these HII regions and the nearest galaxy and their high equivalent widths, it is suggested by the authors that these isolated HII regions represent newly formed regions of star formation where no stars existed previously.

The Hα dots found in the ALFALFA Hα survey in some sense resemble the HII regions discovered in SINGG. In both cases the objects are small and compact and clearly separate from the nearest galaxy. If the Hα dots are determined to be star-forming regions, the question of whether the Hα dots are separate star-forming galaxies or isolated HII regions will be discussed. The distinction between star-forming galaxies and isolated HII regions will be described in Chapter 4.

1.6 Motivation and Goals

The questions of whether or not Hα dots are real emission-line sources and if so what their properties are like is at the heart of this thesis. The Hα dot project began with the discovery of two Hα dot candidates in a single image. In order to answer our questions we will search for additional Hα dot candidates in more images. Once we have found a complete sample of Hα dot candidates we can begin to probe these questions by taking follow-up spectra of the Hα dot candidates. From the follow-up spectra we are able to identify the real emission-line sources, classify them as AGNs or star-forming regions, and measure many of their physical properties.

In Chapter 2 the development of the special software created to search for Hα dots is described. The Hα dot software was run on all the ALFALFA Hα narrowband images in order to find a complete sample of Hα dot candidates as discussed in Chapter 3. In Chapter 4, the motivation for and results of the follow-up spectroscopy of the Hα dot candidates are presented. In Chapter 5, the analysis and results of the narrowband data and spectroscopy will be brought together in order to uncover the nature of Hα dots. Finally, Chapter 6 will summarize the major results and emphasize questions that have risen from the results of this thesis and propose ways in which these questions can be further investigated. Throughout this thesis we have used a Hubble constant of 75 km/s/Mpc.

Chapter 2

Development of Software

2.1 Overview and Goals of Software

The goals of this thesis are to detect, catalog, and understand the nature of Hα dots. In order to figure out what Hα dots are and to study their properties, it is first necessary to find them. The project began with the unexpected discovery of two Hα dots in a single image. It was not known whether more Hα dots existed in other images or if those two objects were the only ones. In order to determine how common Hα dots are, it was necessary to search for more Hα dots. How to carry out this search was not so clear. One way to approach this would be to visually search the continuum-subtracted Hα images in order to find more Hα dots in a similar manner in which the first two were discovered. This seemed like a straightforward way to proceed. However, searching for Hα dots visually leads to several problems. A search based solely on visual inspection is inherently subjective and leads to incompleteness and field-to-field variations that are difficult to quantify. The selection of Hα dots would be more meaningful if it were done in a way in which the completeness of the sample could be quantified.

Finding Hα dots in and of itself is interesting, but finding a statistically complete sample of Hα dots greatly increases the science applications of the survey.

The Hα images from which this survey was to be conducted were taken for an entirely different purpose, to determine the rate of star formation in the local universe. The Hα dot survey was a "spin-off" project. There was no set method or steps to follow for detecting more Hα dots, since their very existence was unexpected. It was necessary to determine an effective method for searching for Hα dots and then write software to implement that method. The method for finding a complete sample of Hα dots was in large part developed through experimentation. We also took advantage of lessons learned from previous emission-line surveys (see section 1.5).

The goal of the software is to identify a complete and objectively-selected list of Hα dots from all of our Hα images. The software identifies, as potential candidates, all objects that have significant Hα emission. The software is designed to be sensitive to very weak sources, in addition to stronger sources. Also, the software is designed to detect emission-line sources regardless of their morphology, so both compact and diffuse sources are detected. It attempts to avoid false detections, objects that are not emission-line sources. After a certain point, the fainter the detection limit is pushed down, the greater the possibility of introducing false detections. The software attempts to push the detection limit as faint as possible, while minimizing the number of false detections. Often false detections can be avoided by visual inspection. Unless there is a specific reason for excluding the source, all sources detected by the script are included in the final catalogue. This final catalogue of Hα dots is then confirmed by followup spectroscopic observations, which will be discussed in Chapter 4. Our ability to determine the nature of Hα dots and understand their role in the universe is dependent on the

completeness of the Hα dot sample. It is critically important that the software is successful in achieving its goals.

In the following sections the details of selecting Hα dots are described. At many points in the development of the software we encountered two or more options in terms of the general methodology and specific details of the selection process. The different choices will be described and the eventual decisions made will be justified. What follows is not only a functional description of how the software works, but an insight into the choices that were made in the development of the software. While the survey method and the software that were established may not represent the very best way to find a complete sample of Hα dots, all the decisions that were made were well thought out and tested. Based on the final Hα dot candidate list and results of the followup spectra, which will be presented in Chapter 3 and 4, the success of the survey can be accessed. The source code of `SuperDot` is included in the appendix.

2.2 The Software Inputs

The software inputs are the fully reduced Hα image, R image, and continuum-subtracted Hα images. Two Hα images and one R image were taken of each field at the WIYN 0.9 meter telescope at Kitt Peak National Observatory. After being reduced in the usual way by bias subtraction and flat field division, the images were cleaned for cosmic rays by an automatic cosmic ray cleaning script. Next the R image was shifted and scaled to the flux level of the Hα images. After the shifting, astrometry was done on the R and Hα images using the US Naval Observatory Astrometry Catalogue. The R image was subtracted from each Hα image and the two resulting continuum-subtracted Hα images were combined.

These fully reduced images, the Hα image, R image, two individual continuum-subtracted Hα images, and combined Hα continuum-subtracted image, are the input into the Hα dot detection script. The script is run once for each field using these 5 images as input.

2.3 SuperDot

`SuperDot`, a program written in the Image Reduction and Analysis Facility (IRAF) scripting language, is run on one field at a time. It is a super script composed of eight special purpose scripts: `dotstart`, `dotmult`, `dotfind`, `dotdel`, `dotadd`, `dotastrom`, `dotphot`, and `dotarith`. `SuperDot` sequentially calls each of the component scripts, each of which performs a specific function. The first script, `dotstart`, sets up the table structure that will be used to store and manipulate information for each field. The first step in the actual processing is to find all of the objects in the image. `Dotmult` finds all the objects in the image by running a finding routine `dotfind` four times, with slightly different parameters targeted at different types of objects. By running `dotfind` multiple times with different parameters, a wider range of objects can be found; however, there are some objects that are found multiple times. In order to delete these duplicate objects a script called `dotdel` is run. Ideally at this point, all the objects in the image should have been found, however to ensure that no objects are missed, `dotadd` displays the image and marks all the objects that are found, so that any objects that are missed can be added manually. Once the x and y pixel positions of all the objects in the image are written into the table, `dotastrom` converts these x and y positions to right ascension and declination. `Dotphot` does photometry on all of the objects in both the R and Hα image. The R and Hα magnitudes and their asso-

ciated errors determined from `dotphot` are written to the table. `Dotarith` selects Hα dot candidates based on the magnitude difference (Hα magnitude minus R magnitude) and the ratio of the magnitude difference to the magnitude difference error. Then each object is inspected visually to ensure that it is a real source.

2.3.1 Dotstart

The purpose of the first script, `dotstart`, is to create the table structure that will be used to organize and store information throughout the rest of the Hα dot detection process, to create an average Hα image, and to measure the total noise in the R image. The table is created and manipulated using the `ttools` package in IRAF. Coordinate information for the field, including the right ascension, declination, and epoch of the observation is read from the header of the image and stored in the header of the table. For the R image, the read noise, gain, average full width at half of the maximum (FWHM) of the stellar profile, and exposure time is read from the image header and written to the header of the table. For the Hα image, the FWHM and exposure time are read from the image header and written to the table. Also, all the columns that will be used to store information and to do calculations are created.

Since there were two individual Hα images taken of each field, the finding routine and photometry could be done on one of the individual Hα images or some combination of the two images. After experimenting with using an individual image, an average image, or a sum of the two images, it was determined that using an average image gave the best results. By averaging the two individual Hα images the signal-to-noise ratio (SNR) of the resulting image is increased. This decreases the possibility of false detections since a spurious source, such

as a cosmic ray, would most likely occur in only one of the images; therefore, the strength of a spurious source would be reduced in the average image. Also, averaging the images increases the possibility of detecting fainter objects. Because of the advantages of using an average image, the two individual Hα images are averaged at the beginning of `SuperDot` and this image is used throughout the rest of the script.

`Dotstart` measures the noise in the R image. The noise in the image is an important input into the next script `Dotfind`, which selects objects that are five sigma above the noise in the image. There are predominately two sources of noise in an image: the Poisson noise from sky photons and the read noise. The Poisson noise is the square root of the number of counts multiplied by the gain. The number of counts is determined using `imstat`, calculating the median value of counts in a long narrow strip of the image. The median is a useful statistical quantity in this circumstance since it is not sensitive to outliers.

The total noise in counts is calculated based on the sky noise and the read noise according to the following formula:

$$\sigma_{tot} = \sqrt{{\sigma_{sky}}^2 + {\sigma_{RON}}^2}. \tag{2.1}$$

After setting up the table structure, calculating the total noise in the image, and writing the appropriate information to the header of the table, `SuperDot` continues on to the next two scripts, `Dotmult` and `Dotfind`, which will find all the objects in the image.

2.3.2 The Finding Algorithm

The purpose of the next two scripts `dotmult` and `dotfind` is to find all the objects in the image. `Dotfind` uses the `daofind` package in IRAF to automatically search the entire image and find all objects that meet a certain set of criteria. `Daofind` finds all objects in the image that have a specified point spread function and are above a specified SNR. `Daofind` is specifically designed to find stellar point-like objects. Many of the objects in the image were, thus, missed since they did not have stellar profiles and were more diffuse and extended.

Based on tests, it was determined that by increasing the FWHM parameter in `daofind` it was possible to find more extended objects. A script called `dotmult` was written to run `daofind` four times with four different values of FWHM, in order to find objects with a range of morphologies from more point-like to more extended shapes. By searching the image multiple times, `dotmult` is able to find a wide range of objects. However there are also many individual objects that are found multiple times. In order to delete these duplicate objects, a script called `dotdel` is run which compares the coordinates of the objects that were found and deletes any detection that lies within a radial separation of two pixels from another detection. In the case of a repeated detection, `dotdel` retains the first detection of the object and deletes any subsequent detections since it is assumed that the centering of the first detection is the most accurate (since it is based on the smaller FWHM criterion).

Tests were also done to determine the appropriate SNR to use as a minimum criterion for selecting objects. A SNR of five was chosen because using a SNR below that introduced a significant amount of noise into the list of detections without including many more real sources. Experimenting with larger SNRs demonstrated

that using a SNR above five caused objects to be missed by the finding routine that appear real when inspected by eye.

The finding algorithm was tested on the R image, the Hα image, and a sum image which combined the R image and the Hα image. It was determined that running the finding algorithm on the sum image resulted in the most objects being found since it has a higher SNR.

The final component of finding all the objects in the image is a script called `dotadd`, which displays the image and places circles around all the objects that have been found. The user can visually inspect the image and add any objects that have been missed. Along with allowing the user the opportunity to add objects that have been missed, `dotadd` provides a good check that the finding routine is working properly. The finding algorithm finds over 99.9 percent of the objects in the image so it is usually only necessary to add one or two objects.

It is important to do a good job finding all the objects in the image. The resulting list of positions is the input for the rest of the software, which does astrometry, photometry, and eventually selects Hα dots. In order to find the most complete sample of Hα dots, it is critical that all the objects in the image are found at this stage in the software.

2.3.3 Astrometry

Once all the objects in the image have been found and their x and y pixel positions have been written to the table, it is necessary to convert those x and y positions on the image to right ascension and declination. Astrometric solutions for the images had been found using the US Naval Observatory Astrometry Catalogue during the previous processing of the images (prior to running the Hα dot scripts).

`Dotastrom` uses `xy2rd` to apply these astronomic solutions and convert from x and y pixel positions to right ascension and declination. Accurate RA and Dec positions in epoch J2000 are written to the table for every detected source.

2.3.4 Photometry

The next major step is to do photometry on all the objects in both the R and Hα images. `Dotphot` uses an aperature-photometry routine called `phot` to compute the instrumental magnitudes of all the objects in both the R and Hα images. Ideally when doing photometry the goal is to measure all the light in the object. This is done by measuring the flux within a given aperature and measuring the background around the source. Choosing the correct aperature size is important when doing photometry. The correct aperature size to use depends on the goal of the project. When doing all-sky photometry, it is important to choose a larger aperature in order to collect all the light from the source. When doing differential photometry it is appropriate to choose a smaller aperature that maximizes the SNR. For a given field, the R and Hα images both have the same FWHM value from the previous processing. Since the goal is to compare the R and Hα magnitudes of each source, the same aperature size was used for a given object in each image. Ideally, the best aperature size would be determined individually for each object in order to do the photometry more accurately. This is practical when doing photometry on several objects, but when doing photometry on hundreds of objects it is not. So the aperature size of five pixels was chosen since it works well for the majority of objects. (One improvement that could be made would be to divide the objects into two groups based on their brightness. Then two different sized aperatures could be used to do the photometry on the brighter and fainter

objects.) Along with measuring the instrumental magnitudes in both filters, `phot` also calculates the magnitude errors. The magnitude errors will be important in the selection of Hα dots. The R and Hα magnitudes and their associated errors are written to the table.

2.3.5 Selecting Hα dots

Hα dots are selected based on two criteria: the magnitude difference and the ratio of the magnitude difference to the magnitude difference error. After photometry is done for all the objects in the image, the magnitude difference is calculated according to the following equation:

$$\Delta m = m_{H\alpha} - m_R. \tag{2.2}$$

For a given object, a magnitude difference of zero indicates that the R magnitude is equal to the Hα magnitude. A positive magnitude difference indicates that the R magnitude of the object is brighter than the Hα magnitude and a negative magnitude difference indicates that the Hα magnitude is brighter than the R. Objects with more negative magnitude differences are potential Hα dot candidates.

The magnitude difference error is calculated based on Hα magnitude error and the R magnitude error as follows:

$$\sigma_{\Delta_m} = \sqrt{{\sigma_{H\alpha}}^2 + {\sigma_R}^2}. \tag{2.3}$$

A good way to measure the significance of the detection is the ratio of the magnitude difference to the magnitude difference error, which is calculated according

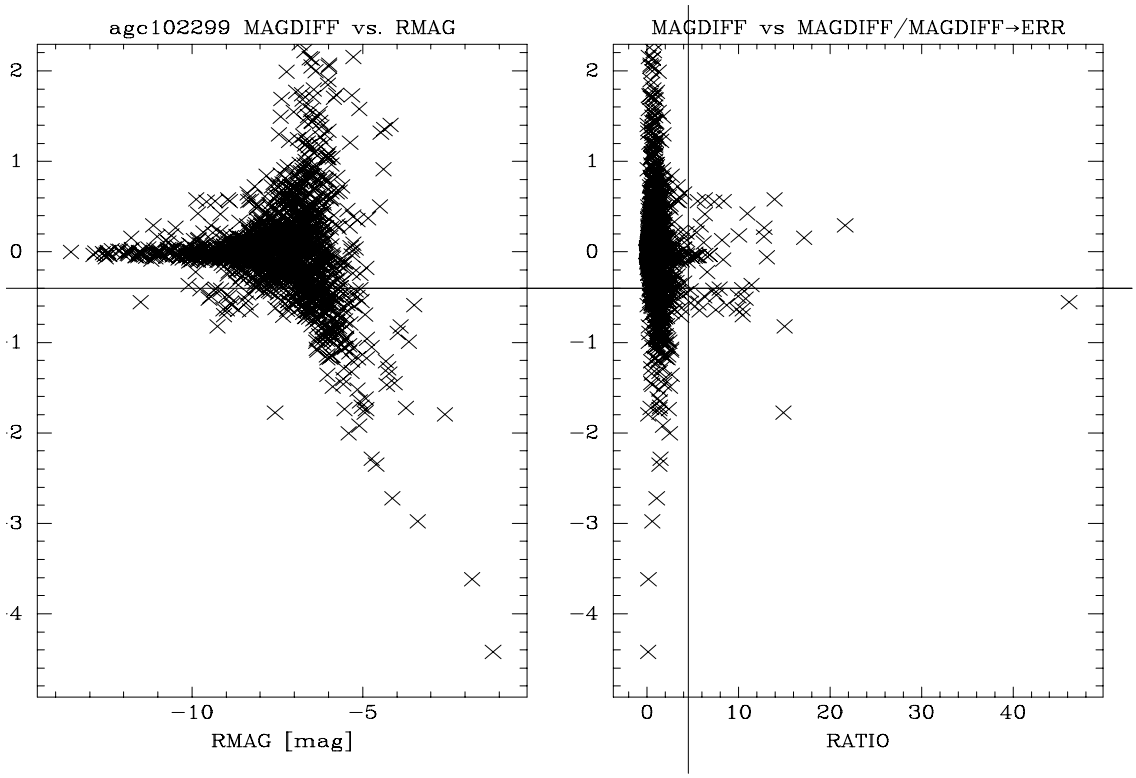

Figure 2.1: Diagnostic Plot of AGC102299. On the left is a plot of magnitude difference versus R instrumental magnitude and on the right is a plot of magnitude difference versus the ratio of magnitude difference to magnitude difference error. The horizontal line indicates a magnitude difference cutoff of -0.4 and the vertical line indicates a ratio cutoff of 4.5. Each 'x' symbolizes an individual object in the image. The objects that are in the lower right hand box with a magnitude difference less than -0.4 and a ratio larger than 4.5 are potential Hα dot candidates.

to the following equation:

$$ratio = \Delta m / \sigma_{\Delta_m}. \tag{2.4}$$

The magnitude difference, magnitude difference error, and ratio are calculated for every object in the field. The two diagnostic plots shown in Figure 2.1 are automatically generated and displayed on the screen. One plot is magnitude difference versus instrumental R magnitude and the other plot is magnitude difference versus the ratio of magnitude difference to magnitude difference error.

Objects with larger ratios and more negative magnitude differences are more likely to be Hα dots. Once the plot is displayed on the screen by `dotarith`, the person running the script is prompted to enter a magnitude difference cutoff and a ratio cutoff. Experimentation was done to determine the appropriate ratio and magnitude difference cutoffs to use. The specific ratio and magnitude difference cutoffs that were used will be discussed in detail in Chapter 3. After the user enters a ratio cutoff and a magnitude difference cutoff, Hα dot candidates are selected that have magnitude differences that are more negative than the magnitude difference cutoff and ratios that are larger than the ratio cutoff.

Once the Hα dot candidates have been selected, each one is automatically displayed so that it can be visually inspected by a person running the script. Localized cut-outs of 200x200 pixel regions around the Hα dot candidates from the R image, Hα image, average continuum-subtracted Hα image, and two individual continuum-subtracted Hα images are displayed as shown in Figure 2.2 and Figure 2.3. The person visually inspects the images and determines if the Hα dot candidate is a real source or a false detection. False detections are usually caused by cosmic rays, saturated stars, or noise in the image. A false detection caused by a cosmic ray can be easily identified since it will appear in only one of the Hα continuum-subtracted images. In order to be considered a real source, the Hα dot must appear in both continuum-subtracted Hα images. Another reason for rejection is a star stump in the R image. Star stumps result from stars being accidently "cleaned" by the cosmic ray cleaning script. The partial subtraction of the star in the R image will cause a large negative magnitude difference. The existence of a star stump can be checked by comparing the pre-cosmic ray cleaned and cosmic ray cleaned R band images of the object. The other common reason for rejection is a false detection caused by a star spike from a saturated star. Hα dot

candidates are also rejected if they are noise. An important criterion in order for the source to be considered real is that it must be visible in the R, Hα, and both Hα continuum-subtracted images. Sometimes corralated noise pixels are selected by the script as Hα dot candidates and these are rejected. In order to distinguish between noise and very faint objects, the images must be inspected closely. Unless there is a specific and clear reason for rejection, the Hα dot candidate is kept.

If the person determines that the source is real, they must next decide if it is an Hα dot or an HII region. The distinction between Hα dot and HII region is based on the immediate environment of the object. An HII region is part of a larger galaxy such as a spiral or dwarf. An Hα dot is an isolated source of Hα emission which is not part of a larger galaxy. Since the script is sensitive to anything that has Hα emission, both HII regions in larger galaxies and Hα dots are detected. It is necessary for the person running the script to distinguish between these two types of objects. The Hα dot candidate is flagged in the final table as a rejection, an HII region, or an Hα dot depending on what the person decides. If it is determined that the object is an HII region or an Hα dot, the finder image of the object is saved.

2.4 The software outputs

The software outputs consist of finder charts and tables that record the results. There are two tables that are created, one large table that contains information on all the objects in the image, and a final table that contains information about only those objects that were selected by `dotarith`. The columns in the table are XCENTER, YCENTER, MAG, SHARPNESS, SROUND, GROUND, FIND, HAMAG, HAMAGERR, RMAG, RMAGERR, MAGDIFF, MAGDIFFERR, RA-

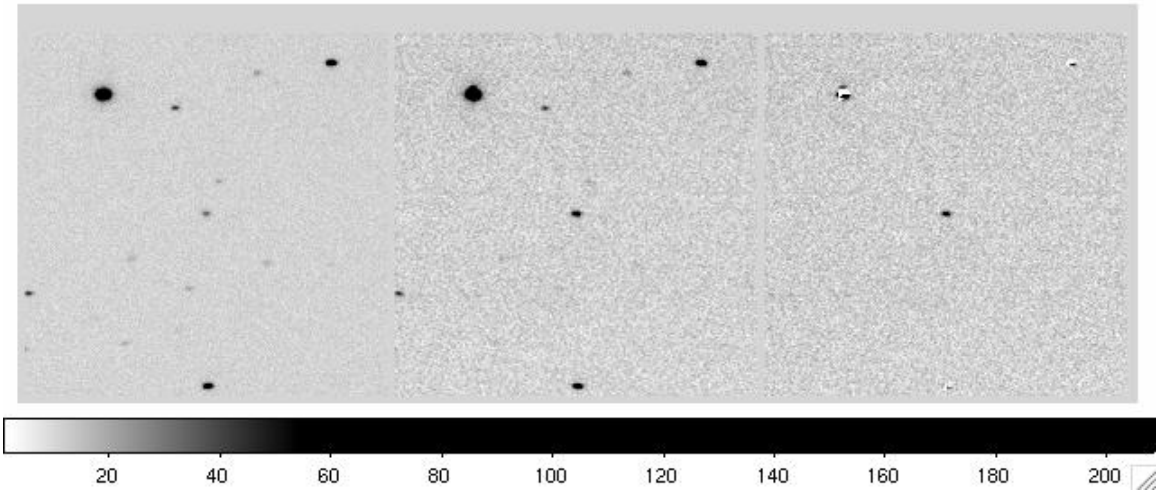

Figure 2.2: My favorite Hα dot - agc2134hadot1. This cutout image is composed of three smaller images: the R, Hα, and Hα continuum-subtracted images (from left to right). Each of these images is a 200 by 200 pixel cutout centered on the Hα dot candidate.

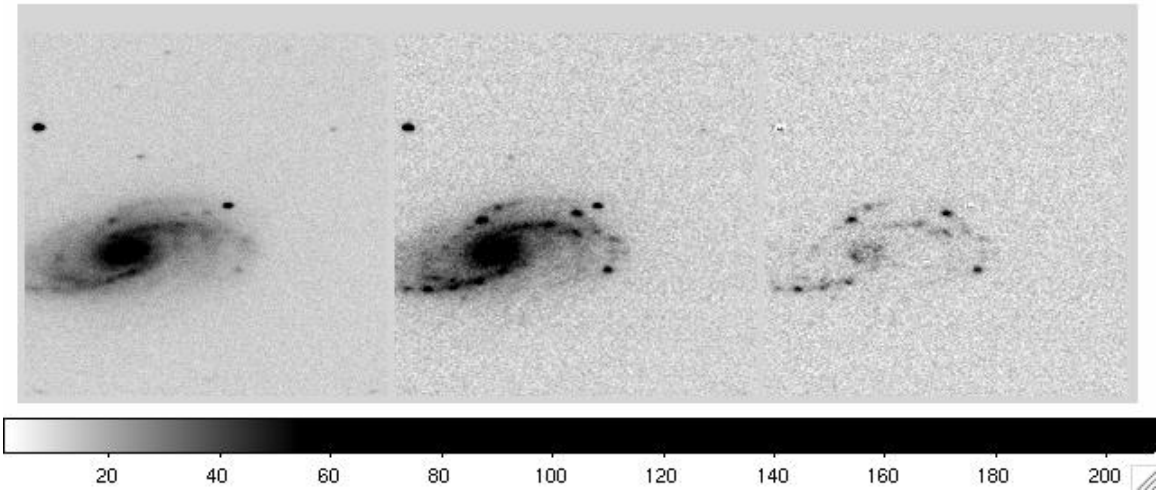

Figure 2.3: This is an HII region in the spiral galaxy AGC2134. This cutout image is composed of three smaller images: the R, Hα, and Hα continuum-subtracted images (from left to right). Each of these images is a 200 by 200 pixel cutout centered on the HII region.

TIO, FLAG, NUMID, RA, DEC, AGCNUM, NAME. XCENTER and YCENTER are the x and y pixel positions of the object in the image. MAG, SHARPNESS, SROUND, and GROUND are information about the magnitude and shape of the object determined by `dotfind`. FIND indicates which run of `dotfind` the object is detected in. `Dotmult` runs `dotfind` four times with gradually increasing values of FWHM. A FIND number of "1" indicates that the object is found in the first run of `dotfind` which is targeted at stellar point-like objects and a FIND number of "2", "3", or "4" indicates that the object is found in the second, third or fourth run of `dotfind`. HAMAG (Hα magnitude), HAMAGERR (Hα magnitude error), RMAG (R magnitude), and RMAGERR (R magnitude error) are the instrumental magnitudes and their errors determined by `dotphot`. MAGDIFF (magnitude difference), MAGDIFFERR (magnitude difference error), and RATIO (the ratio of the magnitude difference to the magnitude difference error) are all calculated by `dotarith` as described above. FLAG signifies the type of source as determined by `dotarith` and the user. A FLAG of "1" indicates an object that is not selected by `dotarith` and a FLAG of "2" signifies an object that is selected by `dotarith` since its magnitude difference and ratio are within the selection area. A unique ID number is assigned to each object in the image and that ID number is listed in the NUMID column. RA and DEC list the right ascension in hours and declination in degrees of each object as determined by `dotastrom`. The name of the ALFALFA field is listed in the AGCNUM column. The objects are listed in order of increasing XCENTER pixel position and information about each object is listed in each of the columns.

In addition to this large table which contains all the objects in the image, a final table which contains only the Hα dot candidates is created. This table contains only those objects that are below the magnitude difference cutoff and

above the ratio cutoff. In addition to containing the same information as the larger table, this FLAG column in the final table indicates whether the object is a rejection (2), HII region (3) or Hα dot (4). For the HII regions and Hα dots, the name of the finder image is listed in the NAME column. Finder images are created and saved for all the Hα dots and HII regions.

`SuperDot` was tested and modified throughout its development. In Chapter 3 the development of the Hα dot candidate list will be discussed and in Chapter 4 the follow-up spectroscopic observations will be described. It should be noted that based on the results of the first follow-up spectroscopic run some improvements to `SuperDot` were made in order to make it more accurate and sensitive. In the next chapter, the usefulness of the software in the development of the final Hα dot catalogue will be described.

Chapter 3

Development of Hα Dot Candidate List

3.1 Overview

The Hα dot software described in Chapter 2 was run on all the narrow-band Hα images obtained for the ALFALFA Hα project in order to develop an Hα dot candidate list. Hα dots are isolated objects that have significant Hα emission. The goal in developing the Hα dot candidate list is to include as many Hα dots as possible while at the same time minimizing the number of false detections. Choosing the criteria by which to select Hα dots is very important since the criteria used will affect the sample. Based on experimentation, certain selection criteria were decided on and used to develop the Hα dot candidate list.

Initially, Hα dot candidates were selected from two fall data sets (September 2006 and October 2007). In order to confirm that the Hα dots are in fact real emission-line sources and determine their nature, it was necessary to take spectra of them. We took spectra of the fall Hα dot candidates at the MDM 2.4 meter

telescope in November 2007. Based on the results of the November 2007 MDM spectra, which will be described in detail in Chapter 4, improvements were made to the Hα dot script and selection method. Then Hα dot candidates were selected from three spring data sets (March 2006, February 2007 and May 2007) using the improved Hα dot script and selection criteria. Spectra were taken of the spring Hα dot candidates in March 2008. The results of the spectra, which will be presented in Chapter 4, suggest that the changes made to the script and selection method between November and March did improve the selection of Hα dot candidates since a larger percentage of the Hα dot candidates that were observed spectroscopically in March are real emission-line sources.

First, the important criteria to consider when selecting Hα dots will be described. Then, the selection method used to initially select Hα dot candidates from the fall data will be discussed. The causes of false detections as determined by the November 2007 spectra will be analyzed. The revised script and selection method used on the spring data will be described. The complete Hα dot catalogue will be presented in Chapter 5.

3.2 Criteria for Selecting Hα Dots

The Hα Dot scripts described in Chapter 2 establish the method for selecting Hα dots and automate a significant portion of the selection process. There are several important decisions that must be made by the user each time the script is run. The user must decide on the magnitude difference and ratio cutoff to be used to select the Hα dot candidates. Then the user visually inspects the Hα dot candidates in order to confirm that they are real and classify them as HII regions or Hα dot candidates.

The magnitude difference, Hα magnitude minus R magnitude, is measured by the Hα dot script for each object in the field. The ratio of the magnitude difference to the magnitude difference error is also calculated. Objects that have more negative magnitude differences are more likely to be emission-line sources since a negative magnitude difference indicates that the object has a brighter Hα magnitude than R magnitude. Also, objects with larger ratio values are more likely to be real Hα dots since a larger ratio value implies a small magnitude difference error relative to the magnitude difference. The ratio value is the equivalent to a signal-to-noise measurement for each object.

Once the magnitude difference cutoff and ratio cutoff are chosen by the person running the script, localized 200 by 200 pixel cutouts of the Hα dot candidate from the R, Hα, and Hα continuum-subtracted images are displayed. We visually inspect each Hα dot candidate to determine if it is a real source or a false detection. In order to be considered a real source the object must appear in the R, Hα, and Hα continuum-subtracted images. When selecting our sample of Hα dots, we attempted to be as inclusive as possible. Hα dot candidates selected by the script are kept unless there is a specific reason for rejection.

If it is a real source, we then classified it as an HII region or an Hα dot candidate. The distinction between HII region and Hα dot candidates depends on the environment around the object and the morphology of the object. If the object is part of a larger galaxy then the object is classified as an HII region. If the object is isolated (clearly outside the outermost isophotes of any galaxy) then it is classified as an Hα dot candidate. The morphology of the object is also considered when deciding whether or not to classify it as an Hα dot candidate. Hα dot candidates tend to be fairly point-like and compact. However, this is not a strict criterion, and objects that appear somewhat extended in the continuum

image can still be included in the sample.

3.3 Running Hα Dot Scripts

3.3.1 The Fall Data

Experimentation was done to determine the magnitude difference and ratio cutoffs to use when selecting Hα dots. Initially the software and selection method was developed using a single field from the September 2006 data, AGC002134, which contained the two Hα dots that were originally noticed by eye. We experimented running the script multiple times on this one field using different magnitude difference and ratio values in order to determine how varying the magnitude difference and ratio cutoffs affected the Hα dot sample.

After experimenting with the individual field, the script was run on the two fall Hα data sets: September 2006 and October 2007. Experimentation was done using different magnitude difference and ratio cutoffs on different fields based on the appearance of the diagnostic plot, which is shown in Figure 2.1 in Chapter 2. The majority of objects lie in the same region in parameter space in the diagnostic plot. On this plot, the potential Hα dots are distinguished from the rest of the objects in the field by having larger negative magnitude differences and higher ratios. It is not clear, however, exactly where to set these dividing lines to select Hα dot candidates. It was eventually determined that using a magnitude difference cutoff near -0.4 and a ratio cutoff near 5 allowed us to select a sample of as many Hα dots as possible without being overwhelmed by false detections. When we ran the script on each field we adjusted these cutoffs slightly depending on the appearance of the diagnostic plot. For example, if there was an object that

had a magnitude difference just larger than -0.4 or a ratio value just smaller than 5, we adjusted the magnitude difference and ratio cutoffs so that the object would be included in the sample.

After the magnitude difference and ratio cutoffs were chosen for each field, the cutout R, Hα, and Hα continuum-subtracted images of every Hα dot candidate selected by the script were inspected visually. The reasons for rejection included saturated stars and noise. Saturated stars were easy to identify. Anything that appeared very faint in the Hα continuum-subtracted image was rejected as noise.

The Hα dot scripts were run on each of 106 15 x 15 arcmin fall fields. For each field, a ratio and magnitude difference cutoff was chosen and the potential Hα dot candidates were inspected visually as described above. The person running the script recorded the results of each field in a log, which included the number of objects that were automatically selected by the script and details about why an object was rejected or whether it was classified as an HII region or Hα dot candidate.

After running the script and applying our selection criteria to 106 fields from the September 2006 and October 2007 data, we found 29 Hα dot candidates. The number of Hα dot candidates varied from field-to-field; some fields had zero, some had one, and a few had two. This sample of Hα dot candidates formed our target list for our first follow-up spectra run at MDM in November 2007.

The results of the follow-up spectra, which will be described in detail in Chapter 4, gave us the opportunity to improve the Hα dot candidate selection method. After analyzing the spectra, it was determined that ten of the 29 Hα dot candidates were not emission-line sources. For each of the false detections, we analyzed the data and looked at the images in detail in order to understand the cause of the false detections. All the false detections were caused by star stumps or cosmic

rays. Star stumps are partially subtracted stars that are accidently "cleaned" by the automatic cosmic ray cleaning script that was run on the images during the initial processing. The cosmic ray cleaning script sometimes confuses stars with cosmic rays and subtracts the center of the star. When this happens to an object in the R image, it causes a false detection since the Hα flux of the object will be larger than the artificially decreased R flux of the object.

In order to decrease the number of false detections, improvements were made to the scripts and the selection method. The first main change that was made was to average the two Hα images at the beginning of the script and to use the average Hα image for the rest of the script, including finding objects and doing photometry. Using an average image has the advantage of improving the SNR. The second improvement that was made was to visually inspect both individual Hα subtracted images in order to prevent false detections caused by cosmic rays. (These two changes could not be implemented on the September data, however, since there is only one Hα image and only one Hα continuum-subtracted image for each field in that data set.) Also, once aware of the star stump problem, we compared the pre-cosmic ray cleaned R image and cosmic ray cleaned R image in order to ensure that the Hα dot candidate was not a false detection caused by a star stump. Other smaller changes to the scripts were also made, mainly to make the scripts more user friendly.

3.3.2 The Spring Data

After making improvements to the scripts and the selection method described above, the Hα dot scripts were re-run on the October 2007 and September 2006 data and run for the first time on three more data sets: February 2007, March

2006, and May 2007. We experimented with using lower ratio cutoffs when selecting Hα dots. Most of the false detections from the November 2007 spectra run had larger ratio values (since they were caused by cosmic rays and star stumps). Also, some of the spectroscopically confirmed Hα dots had ratios that were close to five. So we considered the possibility that maybe we had been excluding potential Hα dots from our sample by setting the ratio cutoff too high. We experimented with re-running the script on some of the October 2007 data using lower ratio values. Some objects that had ratio values below five appeared real when we looked at the images. We decided that the ratio cutoff should be below five, but how low to make it was not clear.

We considered using a data-dependent ratio cutoff that would vary slightly depending on the field-to-field variation. The median ratio value varied slightly from field-to-field. However, since the variation was small, we decided to use a consistent ratio cutoff value on all the fields. Based on tests, we settled on using a consistent ratio cutoff of 4.5 for all the fields.

When visually inspecting the data and selecting our Hα dot candidate list, we were slightly more inclusive than we had been the first time we ran the scripts. A number of objects that satisfied our ratio and magnitude difference cutoffs did not appear at all or appeared very faintly in the images. When we had run the script the first time, we rejected all of these objects. During the second run of the script, we tried to be more inclusive, while at the same time trying to avoid including false detections. Some of the objects we included did not appear at all in the R image and/or were very faint in the Hα continuum-subtracted image. All the images were inspected very carefully, and an object was only rejected if there was a clear reason for rejection. Saturated stars were easy to identify. Cosmic rays only appeared in one of the Hα continuum-subtracted images. Star stumps could

be recognized by comparing the pre-cosmic ray cleaned R image and the cosmic ray cleaned R image. However, it was sometimes difficult to distinguish between noise and very faint sources. In order to be considered an Hα dot candidate the center of the object in the R, Hα and both Hα continuum-subtracted images must be in exactly the same position. As long as this criterion was fulfilled, the Hα dot was kept. We were slightly more inclusive, in terms of keeping more of the very faint sources, when creating the spring Hα dot candidate list than we had been when creating the fall Hα dot candidate list the first time. Each Hα dot candidate was inspected by at least two people in order to ensure that we thought it was a real emission-line source.

The Hα dot scripts were run on 103 fields from the February 2007, March 2006, and May 2007 data. The March 2006 and May 2007 fields are all 15 x 15 arcmin. The February 2007 fields are significantly smaller, 10 x 10 arcmin. After running the script on these 103 fields, we found 32 Hα dot candidates. Two of the 27 spectroscopically confirmed Hα dot candidates, agc200496hadot5 and agc006653hadot1, had ratio values between 4.5 and 5. So decreasing the ratio value selection criteria from 5 to 4.5 increased the number of spectroscopically confirmed Hα dots by 7 percent.

When we ran the revised version of the scripts (that had been run on the Spring data) on the 102 September 2006 and October 2007 fields we found 28 Hα dot candidates. The first and second run of the script on the fall data will be compared in Chapter 5 when the final Hα dot catalogue is presented.

Only six of the 32 Hα dot candidates observed spectroscopically in March were false detections. The false detections were caused by noise or by M stars. Corrolated noise pixels in the Hα image that happened to correspond exactly with the position of an object in the R image caused a couple of false detections.

False detections caused by noise could be reduced in the future by being more careful about accepting very faint sources as Hα dots. The other false detections were caused by M stars. M star spectra have broad absorption troughs in the red part of their spectrum. The resulting low resolution spectrum often causes them to look like emission sources. For example the KISS objective prism survey was very efficient at finding M Stars (Salzer 2000). Since we only have R and Hα observations for the fields there is no way to distinguish between M stars and Hα dots. In order to identify M stars we would need to obtain photometric colors, as was done in KISS to eliminate the M star contaminants (Salzer 2000). Multi-wavelength data is available for some of our fields in the Sloan Digital Sky Survey; however these data are not available for all of our fields.

Even though there were still false detections in the March spectra run (18.8 percent), there were fewer than there had been in the November spectra run (34.5 percent). Also, although slightly less area was searched in the Spring data than the fall data, more Hα dot candidates were found in the Spring data with the revised script than had been found in the Fall data with the old script. This suggests that the improvements to the script not only eliminated most sources of contamination, but also improved the completeness of our Hα dot sample by increasing sensitivity and being more inclusive of very faint sources. So the improvements to the script and selection method did significantly improve our ability to find Hα dots. The final Hα dot catalogue will be presented in Chapter 5.

Chapter 4

What are Hα Dots? : Follow-up Spectroscopy

4.1 Possible Explanations

In order to fulfill our goal of determining the nature of Hα dots and measuring their physical properties, spectra were taken of the Hα dot candidates at the MDM 2.4 meter telescope in November 2007 and March 2008. As described in Chapter 3, all the narrow-band Hα images obtained for the Hα ALFALFA project were systematically searched using the special software described in Chapter 2 in order to find a complete sample of Hα dot candidates. Having found a large sample of Hα dot candidates, we wanted to confirm that they are in fact real emission-line sources. Also, we wanted to determine their nature. Knowing that they exist is interesting by itself, but there is much more that can be learned by taking more observations.

Using a wide-field CCD and narrow-band imaging is an excellent way to identify emission-line objects, however there are inherent ambiguities in narrow-band

imaging. The ambiguities can best be understood through an explanation of how the images were obtained. Images of each field were taken in a narrow-band Hα filter and continuum R filter. The main criterion for selecting Hα dots is that the objects have an excess of Hα flux as compared to the R flux. The images that were searched to find Hα dots were originally taken for an entirely different purpose - to calculate the rate of star formation in the local universe. So the specific wavelength range of the Hα filter was chosen to correspond to the distance of the target ALFALFA galaxy in the field so that the Hα flux and thus star-formation rate of the target galaxy could be measured. Assuming that the Hα dot is at a similar redshift to the target ALFALFA galaxy, the excess Hα flux is indicative of Hα emission, which is corrolated to star formation. However, the Hα dot is not necessarily at the same redshift as the target ALFALFA galaxy. It could be an emission-line object at a higher redshift, such that another strong emission-line such as [O III]λ5007 is redshifted into the Hα filter and shows up as a detection. In order to determine if the Hα dots are low redshift star-forming galaxies or higher redshift background objects it was necessary to take spectra of them.

The spectra will also allow us to distinguish between star-forming regions and active galactic nuclei (AGN). Star-forming galaxies and AGN are both active galaxies that have strong emission lines. They are distinguished from each other based on the dominant source of this activity. If star formation is the dominant source of activity in the galaxy, then it is classified as a star-forming galaxy. If accretion onto a black whole is the dominant source of activity in the galaxy, then it is classified as an AGN. Star-forming galaxies and AGN have different sources of photoionization. The source of photoionization in star-forming galaxies is hot O and B stars. The source of photoionization in AGN is very high energy (hν greater than 100eV) photons (Osterbrock 1989). These different sources of

photoionization produce very different spectra. The energy distribution of stars is predominatly described by a black body curve. Even for hot stars that have a high peak energy, the blackbody curve drops off very quickly toward the blue end of the spectrum. Radiation from stars will not produce the wide range of ionization observed in AGN (Osterbrock 1989). It requires different amounts of energy to ionize different elements. Reaching high ionization states of certain metal atoms takes more energy than ionizing hydrogen and helium. The high energy photons from AGN can ionize metal atoms that can not be ionized by lower energy photons. Photoionization by high-energy photons may remove electrons from inner shells while low energy photons only have enough energy to remove electrons from the outer shell. Therefore emission lines of AGN cover a wide range of ionization including [O III], [S II], [Ne V], and [Fe X]. Observationally, star-forming galaxies can be distinguished from AGN based on the relative strengths of the emission lines. Specifically, the ratio of [N II]λ6583 to Hα and the ratio of [O III]λ5007 to Hβ distinguish star-forming regions from AGN. These emission lines could be measured in our spectra and used to determine whether the Hα dot is a star-forming region or an AGN.

If it is a low redshift star-forming region, the Hα dot could either be an isolated extragalactic HII region or it could be an ultra-low luminosity star-forming galaxy. Isolated HII regions and ultra-low luminosity star-forming galaxies are distinguished based on the morphology, metallicity, and luminosity of the Hα dot. Isolated HII regions look compact in both the Hα continuum-subtracted image and the R image, while star-forming dwarf galaxies appear somewhat diffuse and extended in the R image. Also, from the spectra, the metallicity of the Hα dot can be measured. If, in addition to the morphology criterion, the Hα dot has a high abundance of metals for its luminosity, then it could be an isolated HII region

created with gas that has been tidally stripped from a nearby galaxy. In order to confirm this hypothesis it would be necessary to obtain HI VLA observations in order to determine if there is a tidal HI stream connecting the Hα dot and a nearby larger galaxy. The spectra will be able to help in distinguishing between isolated HII regions and small star-forming galaxies, but will not in all cases be able to give a definitive answer.

Also, from the spectra, we can determine the metallicity and measure the abundances for both the low redshift and high redshift star-forming Hα dot sample. The most abundant elements in a galaxy are hydrogen and helium. The amount of heavy elements, commonly referred to as metals, varies depending on the galaxy. The helium abundance and heavy element abundance in a galaxy are increased as nuclear burning in stars is followed by the return of processed material to interstellar gas (Osterbrock 1989). Elemental abundances in star-forming regions allow us to study the effects of stellar evolution in galaxies and provide insight into the star-formation history of the galaxy. Low-luminosity irregular galaxies with low helium and heavy element abundances are likely to be relatively recently formed objects, so not much processed material has been returned to the interstellar gas (Osterbrock 1989). Another possible explanation for low-luminosity galaxies with low heavy element abundances is that these galaxies have a very low escape velocity so that when supernova explosions of massive stars return heavy elements to the interstellar gas, these heavy elements escape the gravitational attraction of the galaxy and spread out into the intergalactic medium. Therefore, the galaxy appears metal poor since it can not contain its heavy elements. Oxygen is one of the best heavy elements to measure in order to determine the heavy element abundance in star-forming regions. Oxygen is not depleted much by being incorporated into dust particles. Molecular clouds contain dust and metal atoms tend

to attach to dust grains, which are negatively charged. For example, dust attracts carbon and iron. However, Oxygen does not bind to dust and is mainly formed in massive stars (Osterbrock 1989). From the spectra, we will be able to measure the abundances of heavy elements and gain insight into the formation history of the Hα dots.

4.2 Taking the Spectra

Spectra of all the Hα dot candidates were taken at the MDM 2.4 meter telescope in November 2007 and March 2008. Choosing the appropriate grating is important when taking spectra. The grating used affects the wavelength range that is covered and the resolution of individual emission lines. We chose to use a low dispersion grating that allowed us to cover the entire optical spectrum. The grating has 150 lines per milimeter. The spectra are centered at about 5400 angstroms. Spectra taken on both runs covered a range from 3720 angstroms to 7300 angstroms. The reciprocal dispersion of the spectrograph was 3.066 angstroms per pixel. The slit angle was chosen so that it would be close to the parallactic angle, so as to minimize differential atmospheric refraction.

During the five nights of observation in November 2007, all 29 of the fall Hα dot candidates were observed and during the three nights of observation in March 2008, all 32 of the Spring Hα dot candidates were observed. Each Hα dot candidate was observed for at least two separate 20 minute integrations. We chose to do at least two separate observations of each object so that we would be able to confirm whether or not the object was a real emission-line source in cases where the emission lines were so weak that the nature of the object seemed somewhat ambiguous. Having two separate observations also makes it easier to

identify cosmic rays and ensure that cosmic rays are not confused with emission lines. Also, combining two separate 20 minute observations improves the SNR of the spectra and thus improves our ability to make accurate abundance and other types of measurements. The exposure time was chosen to balance our desire to get high quality spectra and to fulfill our goal of observing all the Hα dot candidates at least twice.

Since many of the Hα dot candidates are very faint, we could not always see the object in the slit and therefore we had to do blind offsets from nearby bright stars. We moved the telescope to a bright star near the Hα dot candidate and then centered the bright star in the slit. We then offset the telescope a known amount to the Hα dot candidate. Sometimes we could see the Hα dot candidate in the slit, but sometimes we could not see it, since it was so faint. This procedure of doing small blind offsets worked well and we were successful at getting all the Hα dot candidates in the slit.

While at the telescope, we looked carefully at the raw spectra of the Hα dots and decided which were most interesting and for which it would be useful to obtain additional integrations. After we had finished observing each Hα dot candidate twice we returned to the most interesting Hα dots and took additional observations. The ones we took longer observations of were those that appeared to have strong emission-lines and for which we thought longer observations would improve our ability to obtain accurate abundances.

Calibration images, including internal flat lamps, twilight flats, Hg-Ne comparison lamps, and biases were taken. We also observed standard stars throughout each night. Only a small amount of observing time was lost to clouds.

4.3 Spectroscopic Reductions

The November 2007 spectra were reduced using IRAF. Pixel-to-pixel variation was removed from the spectra by dividing by an averaged-combined internal flat lamp image. Based on tests, it was determined that it was best not to use the bias images because of an unusual and variable noise pattern that was present in them, so no bias correction was done. A one-dimensional spectrum was extracted from the two-dimensional image. Cosmic rays were removed from the object spectra using a program called `Lacos_Spec` (van Dokkum 2001) . The spectra were then wavelength calibrated using the Hg-Ne comparison lamp spectra, and flux calibrated using a sensitivity function derived using the standard star observations.

4.4 Results of Spectroscopy

4.4.1 Results from the November MDM Spectra

We obtained spectra of all 29 fall Hα dot candidates in November 2007 at the MDM 2.4 meter telescope. Ten of the 29 Hα dot candidates were not emission-line sources. After looking closely at the original narrow-band data, it was determined that these false detections were caused by cosmic rays and star stumps (as described in Chapter 3). Of the 19 real emission-line sources, eight are background objects (42 percent) and eleven are low redshift ultra-low-luminosity, star-forming galaxies (58 percent). The low redshift star-forming galaxies were all detected by the Hα emission line. The background objects are at different redshifts depending on the emission line by which they were detected. The majority of the high redshift Hα dots (7) were detected by [O III]λ5007. One of the high redshift Hα dots was detected by Mg IIλ2798.

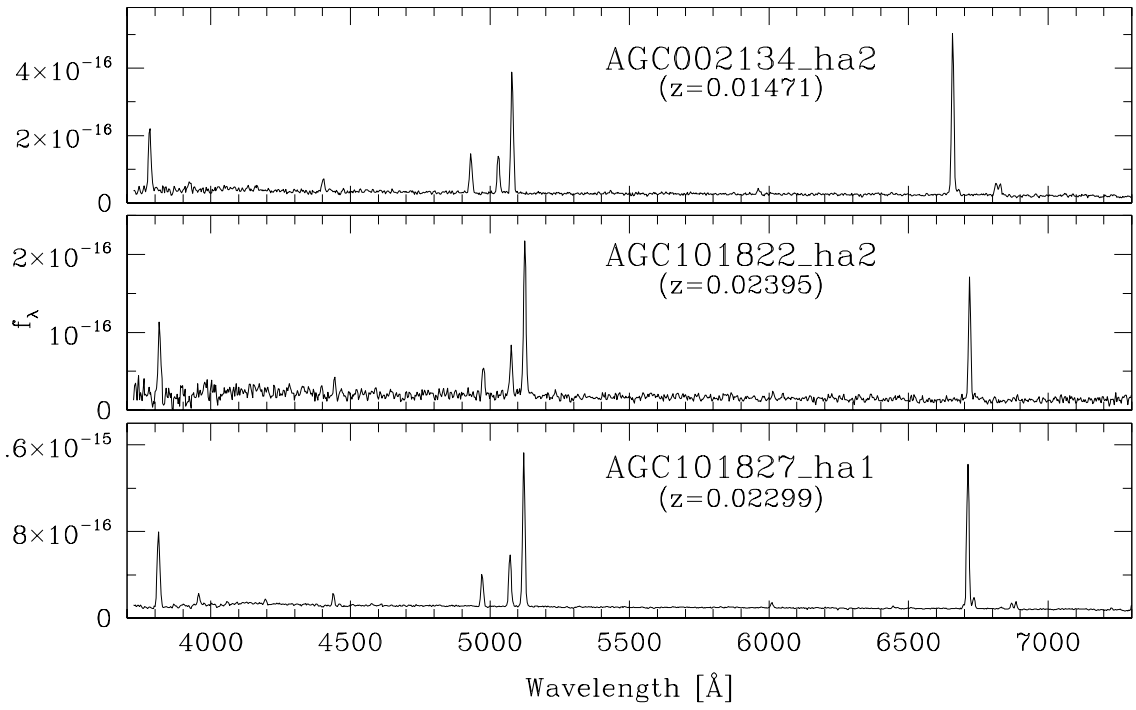

Figure 4.1: Example spectra of low redshift Hα dots.

Figure 4.1 shows example spectra of low redshift Hα dots that were detected by the Hα emission line. Figure 4.2 shows example spectra of high redshift Hα dots that were detected by the [O III] λ 5007 emission line. Figure 4.3 shows an example spectrum of a quasar that was detected by the [Mg II] emission line. Figure 4.5 shows example spectra of two false detections caused by M stars.

The specific redshift of each Hα dot is measured from the spectra. When an electron makes a transition between two different energy states in an atom it releases a discrete amount of energy, which corresponds to a specific wavelength. Based on quantum mechanical calculations and earth based experiments, the rest wavelengths that correspond to different atomic transitions have been determined. From our spectra, we can identify certain emission lines and measure the wavelength at which these emission lines occur. Due to the expansion of the universe

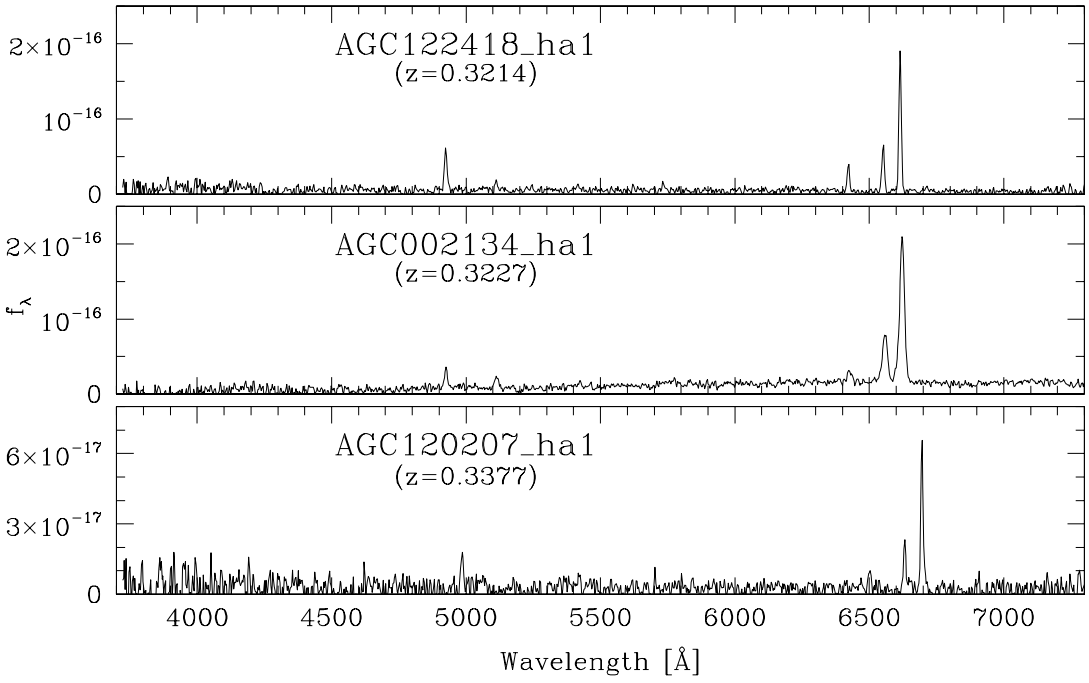

Figure 4.2: Example spectra of high redshift Hα dots.

most galaxies are moving away from us and therefore their light is shifted to longer wavelengths. The redshift defined by the following formula is measured for each Hα dot:

$$z = \frac{\lambda_{observed} - \lambda_{rest}}{\lambda_{rest}}. \tag{4.1}$$

In order to distinguish star-forming galaxies from AGN, the relative strengths of the emission lines for each of the 19 Hα dots were measured. Specifically, by measuring the ratio of [N II]λ6583 to Hα and [O III]λ5007 to Hβ star-forming regions can be distinguished from AGN. The Hα dots are plotted on a diagnostic plot in Figure 4.4. Star-forming regions are distinguished from AGN using a theoretical model described by Dopita and Evans (1986). In Figure 4.4, the curve shows the theoretically predicted arc along which galaxies in which star formation

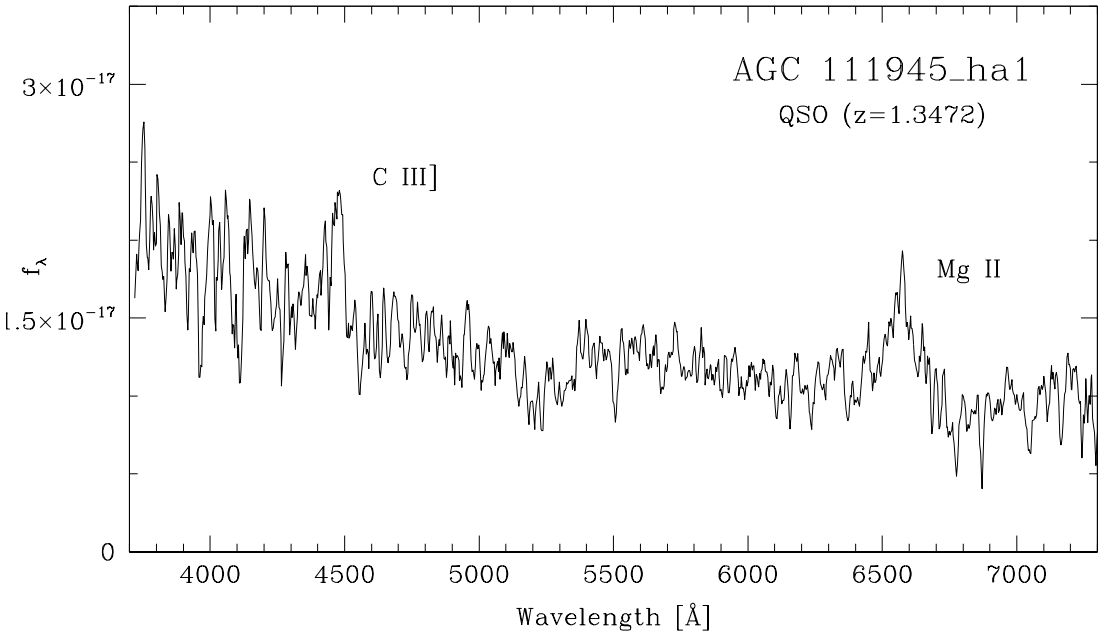

Figure 4.3: Example spectra of a quasar detected by the Hα dot survey.

is the dominant source of activity are expected to lie. Objects that do not lie along this arc are considered to be AGN. Both the low redshift and high redshift Hα dots are plotted on this line diagnostic diagram. Based on the diagram, all the low redshift Hα dots appear to be star-forming regions since they lie close to the theoretically predicted arc.

For the high redshift Hα dots, star-forming regions and AGN can not be definetively distinguished based on our current data. The high redshift Hα dots were detected by [O III]λ5007 or other strong emission lines that lie further towards the blue end of the spectrum. Because of the wavelength coverage of our spectrograph and the redshift of these background objects, we did not cover the part of the spectrum necessary to detect the [N II]λ6583 and Hα lines for these objects. However, we can make an educated guess about whether the high redshift object is an AGN or a star-forming region based on the ratio of [O III]λ5007 to

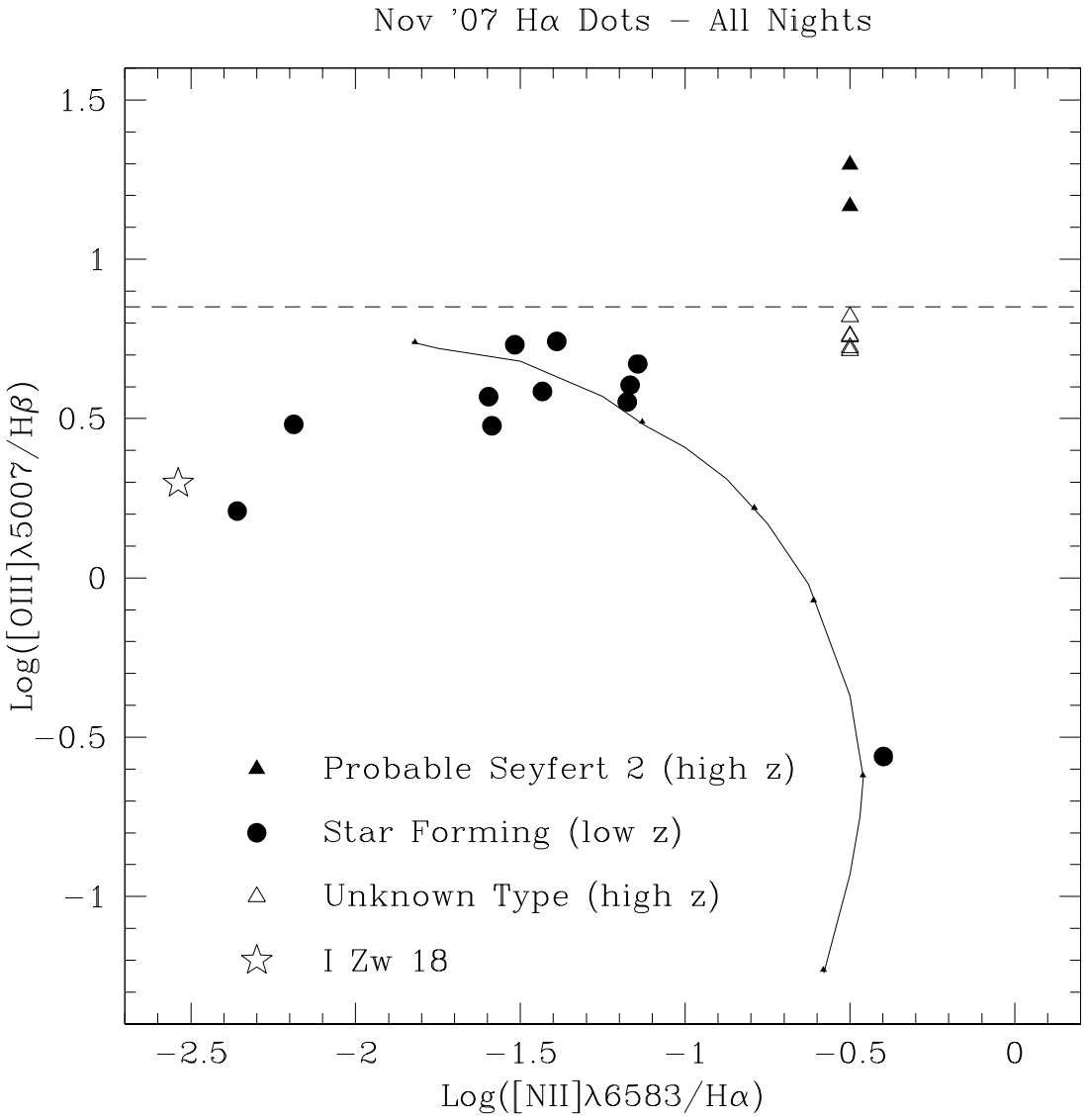

Figure 4.4: Emission-line ratio diagnostic diagram for the November 2007 Hα dots. All circles and triangles indicate Hα dots. The star indicates the placement of I Zw 18 on the diagnostic diagram. (1 Zw 18 is not an Hα dot and is plotted here only for reference purposes.) The high z Hα dots do not have a log([N II]λ6583/Hα) measurement and are plotted with a default value of -0.5. The dashed line represents the division between Seyfert galaxies and star-forming regions for the KISS high z sample.

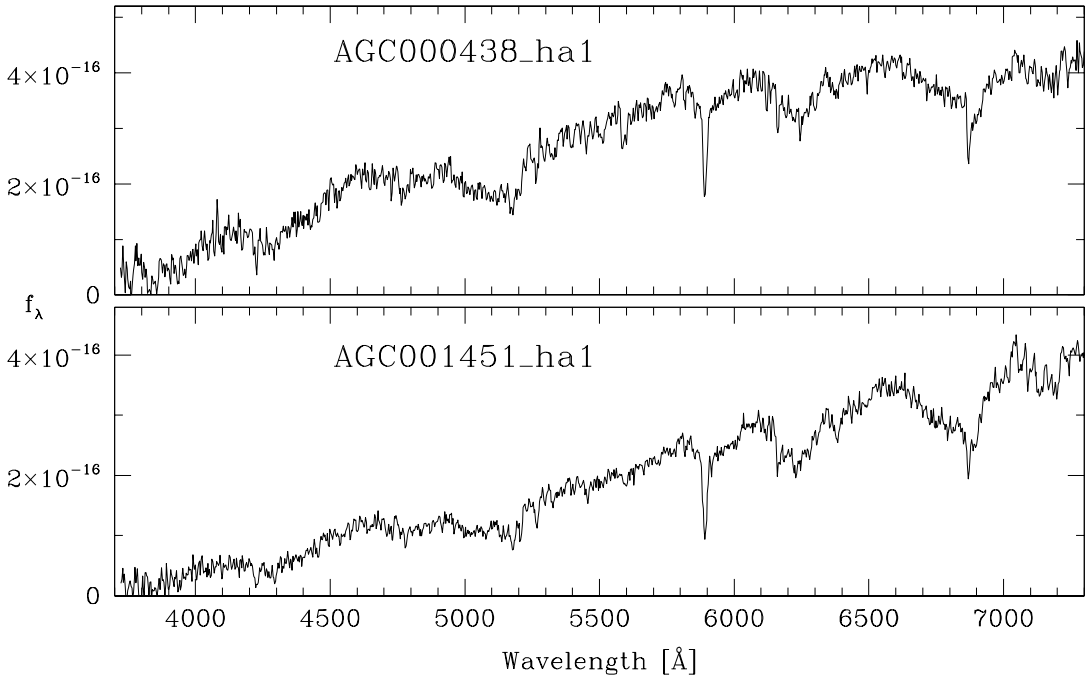

Figure 4.5: Example spectra of Hα dots candidates that were determined to be false detections. One of the most common causes of false detections is M stars, which are shown in this Figure.

Hβ. Based on the KISS high redshift sample, galaxies that have a value of log([O III]λ5007/Hβ) above 0.85 are likely to be AGN and galaxies below 0.85 are likely to be star-forming (Salzer, private communication). Although this cutoff is not necessarily true for the high redshift Hα dot sample, it provides a useful guideline. If we take more spectra that cover the red end of the high redshift galaxies, we will be able to measure the [N II]λ6583 and Hα emission lines and distinguish AGN from high redshift star-forming galaxies. By doing this we will be able to study the properties of star-forming galaxies at a redshift of about 0.32 in more depth.

Also, based on the diagnostic plot, the metallicity of the star-forming Hα dots can be measured. The metal poor star-forming galaxies lie on the upper part of the

curve, while the metal rich star-forming galaxies lies on the lower part of the curve. The majority of the star-forming Hα dots are metal poor (91 percent). As will be described in more detail in Chapter 5, the Hα dots tend to be low luminosity. Low-luminosity galaxies tend to be metal poor because low luminosity implies low mass and low mass galaxies are less likely to be able to keep their metals from escaping in the supernova explosions.

Two of the Hα dots, agc120207ha2 and agc100381ha1, are extremely metal poor. The discovery image of AGC120207ha2 is shown in Figure 4.2. The abundance of heavy elements in a galaxy increases as more stars are formed and die and enrich the gas. Therefore, a very low abundance of heavy elements suggests that star formation has just recently begun in these two galaxies. Star-forming regions are probably formed when the collision of two or more lower density HI clouds result in a higher density HI cloud which begins to form O stars (Osterbrock 1989). Since these two Hα dots are so metal poor it is likely that the gas has just recently become dense enough for star formation to begin and we are seeing the early episodes of star formation in these recently formed Hα dots. Another possibility is that because these Hα dots are so low luminosity and thus very low mass, they have been unable to retain their heavy elements. So over time as stars form and produce heavy elements, these heavy elements escape into the intergalactic medium resulting in a star-forming galaxy that appears metal poor despite having a long star formation history. One way to distinguish between these possibilities would be to measure the abundance of heavy elements in the intergalactic medium surrounding the Hα dots. However, this is difficult to do observationally. One way to measure the heavy element abundances in the intergalactic medium is by looking at absorption lines of quasars in high resolution x-ray spectroscopy (Kilgard, private communication). Unfortunately the

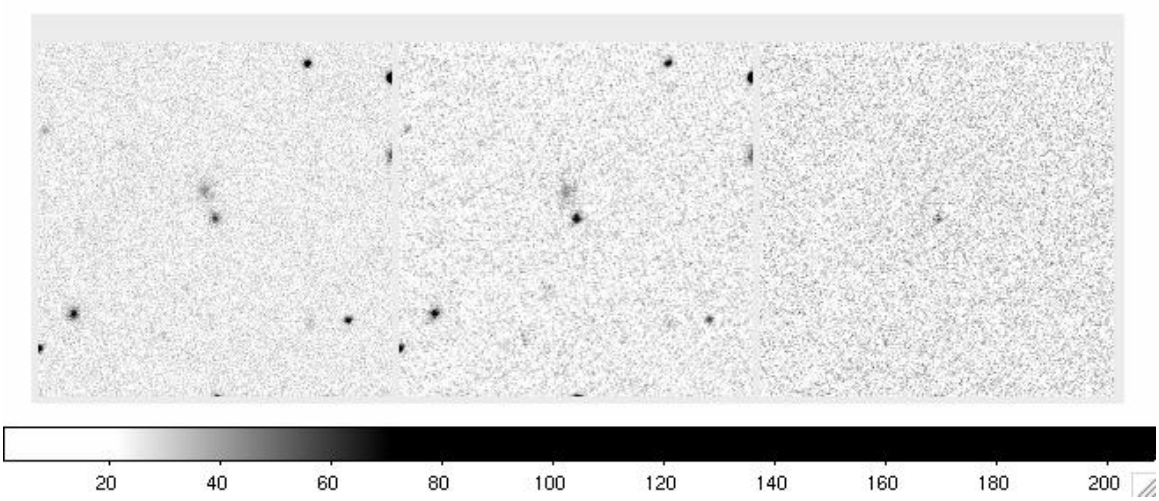

Figure 4.6: AGC120207ha2 is an example of an extremely metal poor Hα dot.

coincidence of a bright quasar adjacent to an Hα dot is expected to be rare.

The galaxy I Zw 18 is shown on the Hα dot diagnostic plot for comparison. I Zw 18 is one of the most metal-poor galaxies that is known in our universe. While the two extremely metal poor Hα dots mentioned above are not quite as metal-poor as 1 Zw 18 they are in a similar range. The fact that two of the 11 low redshift Hα dots we obtained spectra of in November 2007 are extremely metal poor indicates that the Hα dot survey is sensitive to and very successful at finding metal poor objects.

Table 4.1 presents the physical properties mentioned above for each of the 19 spectroscopically confirmed November 2007 Hα dots. The first column gives the name of the Hα dot. The next two columns list the log value ratios of different emission lines - [O III] / Hβ and [N II] / Hα. The fourth column lists whether the Hα dot is a lower redshift object (LZ) at the same redshift as the target ALFALFA galaxy or a higher redshift (HZ) background object . The fifth column lists the galaxy type as determined from the diagnostic diagram based on the relative strengths of the emission lines. SF indicates star-forming region, Sy2

Table 4.1: November Spectroscopic Results

Name	[O III]/Hβ	[N II]/Hα	Type1	Type2	z	Vel	σ_{vel}	Log(O/H)+12
(1)	(2)	(3)	(4)	(5)	(6)	(7)	(8)	(9)
AGC332915ha1	0.6053	-1.1670	LZ	SF	0.02083	6245	22	8.07
AGC332912ha1	1.1673	-0.5000	HZ	Sy2	0.32289			
AGC000438ha3	0.5687	-1.5965	LZ	SF	0.01710	5126	27	7.88
AGC111945ha1	-9.9900	-9.9900	HZ	QSO	1.3472			
AGC332921ha1	0.5526	-1.1754	LZ	SF	0.02398	7190	24	8.07
AGC110790ha1	0.7231	-0.5000	HZ	??	0.33879			
AGC110790ha3	0.7567	-0.5000	HZ	??	0.33954			
AGC120207ha1	0.8196	-0.5000	HZ	??	0.33768			
AGC120207ha2	0.4816	-2.1877	LZ	SF	0.01830	5485	30	7.61
AGC002026ha1	-0.5603	-0.3983	LZ	SF	0.01766	5294	26	9.03
AGC122418ha1	0.7140	-0.5000	HZ	??	0.32140			
AGC100381ha1	0.2100	-2.3592	LZ	SF	0.01719	5154	27	7.53
AGC001250ha1	0.7602	-0.5000	HZ	??	0.33916			
AGC002134ha1	1.2972	-0.5000	HZ	Sy2	0.32272			
AGC002134ha2	0.4777	-1.5864	LZ	SF	0.01471	4408	22	7.88
AGC332951ha1	0.7319	-1.5170	LZ	SF	0.00936	2805	20	7.92
AGC101822ha2	0.7423	-1.3894	LZ	SF	0.02395	7180	33	7.97
AGC102270ha1	0.5848	-1.4329	LZ	SF	0.01726	5174	23	7.95
AGC101827ha1	0.6715	-1.1441	LZ	SF	0.02299	6892	17	8.10

indicates Seyfert 2 galaxy and QSO indicates quasar. For several of the objects we were not able to determine the type because we do not have the necessary emission-line ratios. The objects for which we are unsure of their designation are marked with question marks. In the future, when we obtain more spectra of these objects, we will be able to determine their type. Column 6 lists the redshifts of the Hα dots. The velocity and its associated error are shown in columns 7 and 8. The velocity from the optical spectra is an average obtained by computing the redshift for each of the stronger emission lines separately. Most of the time Hβ, Hα, [O III] 5007, [O III] 4959, and any other lines that are sufficiently strong are used to make the velocity calculation. The velocity has only been calculated for the low redshift Hα dots. Column 9 lists the abundances of the low redshift Hα dots. The abundances were calculated using the "coarse abundance" method detailed in Salzer 2005. The abundances are accurate to 0.15 - 0.20. In the future we will be able to calculate more accurate abundances. These abundance provide useful information about the chemical composition of the Hα dots.

4.4.2 Results from the March MDM Spectra

All 32 spring Hα dot candidates were observed spectroscopically in March 2008 at the MDM 2.4 meter telescope. Six of the Hα dot candidates (18.8 percent) are not real emission-line sources. This is a significant improvement as compared to the number of false detections (34.5 percent) in the initial November 2007 spectra run. This decrease in the number of false detections is a result of the detailed analysis of the false detections from the November spectra and subsequent improvements to the Hα dot software and selection method (as described in Chapter 3).

Based on the spectra, 26 of the Hα dot candidates are confirmed to be real emission-line objects. Similar to the November spectra results, the Hα dots are a combination of low redshift objects (16) and high redshift objects (10). The majority of the high redshift objects were detected by the [O III]λ5007 emission line. Two of the high redshift Hα dots (AGC200598_hadot4 and AGC010176_hadot1) are quasars that were detected by C IV λ1549. These two quasars are at a redshift of about 3.3. This suggests that our Hα dot selection method is sensitive enough to find very high redshift quasars in addition to finding nearby low-luminosity star-forming regions.

At the time of writing this thesis, we are still in the process of reducing the March 2008 spectra. Once we finish reducing the spectra, we will be able to measure redshifts, lines ratios, and distinguish between star-forming regions and AGN as was done for the November 2007 spectra.

4.5 Concluding Remarks

We have derived a great deal of information about the nature of Hα dots from their spectra. We have identified the real emission-line sources and measured their

physical properties - including emission-line ratios, redshifts, and velocities. For most of the Hα dots we have determined whether they are star-forming regions or AGN. In Chapter 5, we will bring together these physical properties measured from the spectra with an analysis of the photometric and morphological properties of the Hα dots obtained from the narrowband image data - including volume density, projected distances, luminosities, and star formation rates. Thus we will be able to develop an even deeper understanding of the nature of Hα dots.

Chapter 5

Results of Survey and Science Applications

5.1 Catalogue Process Results

The revised Hα dot software and selection method was run on all ALFALFA Hα narrow-band images from the 5 observing runs. The ALFALFA Hα narrow-band images can be broken into two large data sets: the fall data and the spring data. The Hα dot software was run on the fall data twice. After the first time the software was run on the fall data and the results of the fall follow-up spectroscopy were analyzed, revisions were made to the software. In addition to running the revised software on the spring data, the revised software was also re-run on the fall data. Because the software, selection limits, and visual inspection methods had been revised, the results of the first run of the software on the fall data are not retained. The discrepencies between the first and second run of the software on the fall data are discussed below.

The script was run on a total of 205 fields. After running the script on all the

fields, 60 Hα dot candidates were found. The number of Hα dot candidates varied from field-to-field. Some fields have zero Hα dot candidates, some have one, and a few fields have two or more Hα dot candidates.

Details of the Hα dot candidates are shown in Table 5.1. The first column is a running number from 1 to 60. The second column lists the name of the Hα dot candidates. The next two columns list the RA and Dec (epoch J2000). The fifth column lists the magnitude difference, which is calculated by `superdot` as described in Chapter 3, by subtracting the R magnitude of the object from the Hα magnitude of the object. A positive magnitude difference indicates that the R magnitude is greater than the Hα magnitude; a magnitude difference of zero indicates that the R magnitude is equal to the Hα magnitude; and a negative magnitude difference indicates that the Hα magnitude is greater than the R magnitude. The sixth column lists the ratio of the magnitude difference to the magnitude difference error, which is also calculated by `superdot` as described in Chapter 3. The ratio value is similar to a measure of the SNR of a detection. A larger ratio value indicates a more significant detection. Hα dot candidates are initially selected based on their magnitude difference and ratio values. Objects with more negative magnitude differences and larger ratio values are more likely to be real Hα dots. Once the selection criteria has been chosen, each Hα dot is inspected visually in order to decide whether or not it should be classified as a real Hα dot.

Much experimentation was done to determine the appropriate magnitude difference and ratio cutoffs to use. Initially, in the fall, a ratio value of 5 was chosen when selecting Hα dot candidates. These fall Hα dot candidates were observed at MDM in November 2007. We then analyzed the results of the November 2007 spectra as described in Chapter 4. Some of the spectroscopically observed fall

Table 5.1: Hα dot Candidates

Row	Name	RA (hours)	DEC (degrees)	magdiff (mag)	ratio	spec?
(1)	(2)	(3)	(4)	(5)	(6)	(7)
1	agc001292_hadot1	1:50:37.7	27:33:43	-0.681	10.574	No
2	agc002134_hadot1	2:39:04.2	27:52:37	-1.237	19.508	Yes
3	agc002134_hadot2	2:38:50.1	27:47:43	-1.208	34.167	Yes
4	agc002134_hadot3	2:39:12.6	27:52:02	-1.073	4.527	No
5	agc102268_hadot2	0:42:55.6	25:51:26	-0.647	5.769	No
6	agc102270_hadot2	0:45:14.2	27:27:14	-0.498	9.503	Yes
7	agc111945_hadot1	1:44:47.3	27:16:39	-0.633	4.761	Yes
8	agc122418_hadot1	2:34:34.2	27:16:54	-1.408	5.595	Yes
9	agc332912_hadot2	23:11:56.1	27:22:12	-0.608	10.539	Yes
10	agc100381_hadot2	0:38:16.1	26:59:31	-0.485	8.258	Yes
11	agc100489_hadot1	0:43:52.5	26:08:57	-0.499	6.519	No
12	agc101822_hadot1	0:40:38.0	27:02:30	-1.752	4.884	No
13	agc101822_hadot3	0:40:54.3	26:57:21	-0.482	14.091	Yes
14	agc101826_hadot1	0:47:13.2	26:40:22	-0.444	4.616	No
15	agc101827_hadot1	0:49:44.9	27:07:52	-0.846	56.908	Yes
16	agc110790_hadot1	1:44:40.3	27:54:35	-2.012	4.830	Yes
17	agc110790_hadot5	1:44:46.0	28:03:03	-0.665	5.854	Yes
18	agc120207_hadot1	2:24:01.6	25:28:17	-1.620	5.410	Yes
19	agc120207_hadot2	2:23:33.2	25:32:43	-0.419	5.853	Yes
20	agc122211_hadot1	2:31:01.6	26:33:23	-1.378	4.521	No
21	agc1250_hadot1	1:47:12.8	28:01:38	-1.664	5.203	Yes
22	agc1955_hadot1	2:28:33.7	25:19:51	-0.530	5.802	No
23	agc331266_hadot1	23:40:54.0	27:27:21	-0.599	4.518	No
24	agc332915_hadot2	23:18:43.1	26:13:36	-0.844	21.528	Yes
25	agc332921_hadot1	23:21:17.8	27:54:32	-0.559	18.340	Yes
26	agc438_hadot1	0:41:40.3	25:26:52	-0.917	4.530	No
27	agc438_hadot2	0:41:02.7	25:27:42	-0.519	19.275	Yes
28	agc573_hadot2	0:55:43.2	24:16:51	-0.592	4.709	No
29	agc005454_hadot1	10:06:51.7	12:37:31	-0.505	8.604	Yes
30	agc200598_hadot2	10:48:38.0	12:17:08	-1.136	5.583	Yes
31	agc200598_hadot3	10:48:55.2	12:10:52	-0.935	6.173	Yes
32	agc200598_hadot4	10:49:06.8	12:16:50	-0.492	6.212	Yes
33	agc211006_hadot1	12:01:23.7	14:00:40	-1.873	6.367	Yes
34	agc007817_hadot1	12:39:00.4	13:23:55	-1.592	6.803	Yes
35	agc182483_hadot1	8:47:17.9	10:02:33	-1.635	90.693	Yes
36	agc182483_hadot2	8:47:15.3	10:02:30	-1.111	30.521	Yes

Continued on next page

Table 5.1 – continued from previous page

Row	Name	RA (hours)	DEC (degrees)	magdiff (mag)	ratio	spec?
(1)	(2)	(3)	(4)	(5)	(6)	(7)
37	agc182483_hadot3	8:47:17.6	10:02:37	-1.012	19.874	Yes
38	agc182483_hadot4	8:47:08.5	10:10:36	-0.608	5.466	Yes
39	agc200496_hadot1	10:37:11.3	12:07:48	-2.369	5.431	Yes
40	agc200496_hadot5	10:37:09.5	12:14:57	-0.777	4.732	Yes
41	agc200496_hadot7	10:36:59.6	12:06:08	-0.551	7.610	Yes
42	agc215158_hadot1	11:40:48.8	13:07:40	-0.717	9.473	Yes
43	agc220201_hadot1	12:12:37.8	11:03:29	-0.420	4.807	Yes
44	agc220292_hadot1	12:16:55.3	12:50:06	-0.594	13.769	Yes
45	agc223205_hadot1	12:50:55.3	12:01:31	-0.732	18.794	Yes
46	agc8114_hadot1	12:59:59.9	13:36:45	-0.574	14.222	Yes
47	agc006653_hadot1	11:41:19.7	16:03:22	-0.444	4.979	Yes
48	agc006666_hadot1	11:41:55.6	15:56:36	-0.683	8.483	Yes
49	agc009330_hadot1	14:30:43.9	13:57:08	-0.581	25.649	Yes
50	agc010176_hadot1	16:05:21.8	13:42:05	-0.492	15.458	Yes
51	agc010384_hadot1	16:26:44.2	11:37:46	-1.333	10.277	Yes
52	agc010384_hadot2	16:27:04.6	11:37:48	-0.857	13.778	Yes
53	agc010384_hadot4	16:26:43.8	11:37:52	-0.753	7.677	Yes
54	agc010384_hadot5	16:26:53.6	11:39:09	-0.618	96.515	Yes
55	agc010384_hadot6	16:26:22.7	11:29:04	-0.424	8.195	Yes
56	agc230859_hadot1	13:57:05.3	14:04:51	-1.501	23.887	Yes
57	agc242319_hadot1	14:05:24.6	12:10:16	-0.477	6.980	Yes
58	agc242319_hadot2	14:04:57.9	12:09:19	-0.409	10.121	Yes
59	agc260281_hadot1	16:08:37.2	11:59:01	-1.372	20.289	Yes
60	agc262397_hadot1	16:04:17.0	11:37:33	-0.535	18.025	Yes

Hα dot candidates were not real emission-line sources. After analyzing the false detections, we then revised the software and selection method as described in Chapter 3. In addition to making improvements to minimize the number of false detections, we also increased the sensitivity of the software so that it would be able to detect fainter Hα dot candidates. We lowered the ratio cutoff from 5 to 4.5. As can be seen in Table 5.1, 12 of the 60 Hα dot candidates have ratio values below 5. Lowering the ratio cutoff increased the sample size by 20 percent!

The final column lists whether or not a follow-up spectrum has been taken for each Hα dot candidate. Spectra were taken of all the spring Hα dot candidates in March 2008 at MDM. Also, spectra were taken of all the fall Hα dot candidates (from the first run of the software on the data) in November 2007 at MDM. When the revised script (that had been run on the Spring data) was re-run on the fall data, several new Hα dots were found that had not been detected previously and so no spectra have yet been taken of these objects as indicated by the word "No" in column 7 in Table 5.1. Eleven of the Hα dot candidates have not yet had spectra taken of them. All 11 of these Hα dot candidates are new detections from the fall data set. Seven of the 11 new fall Hα dot candidates have ratio values below 5. The remaining 4 new fall Hα dot candidates are within our original selection criteria and were rejected previously because they appeared very faint in the Hα subtracted image or come from the few fields that were skipped during the original fall Hα dot selection.

None of the false detections from the original fall Hα dot candidate list were re-detected when the revised Hα dot script was run on the fall data. One of the goals of the revised Hα dot script and selection method is to minimize the number of false detections. The main change that was made was visually inspecting all the images carefully in order to exclude cosmic rays and star stumps (the main causes of the false detections). We emphasize that no reference was made to the results of the fall spectroscopy when running the revised script on the fall data, so had one of the false detections been re-selected, it would appear in this list. This is not to say that there are no false detections remaining in the fall data set. Some of the newly selected Hα dots that have not yet had spectra taken of them may in fact end up being false detections.

Another difference between the results of the first and second runs of the

software on the Hα data is that two fall Hα dot candidates AGC332951_ha1 and AGC2026_ha1 that had been classified as Hα dot candidates originally have now been re-classified as HII regions within a larger galaxy. Both these objects are clearly extended in the R and the Hα image. By re-classifying these two objects, we are being more consistent with our definition of an Hα dot as compact and isolated.

One interesting Hα dot to notice is AGC2134_ha3. As mentioned in Chapter 1, the field AGC2134 was the first field in which we initially noticed Hα dots by eye in the images. When we looked at the Hα continuum-subtracted image we noticed two distinct points of Hα emission that are clearly separate from the spiral galaxy in the field (AGC2134_ha1 and AGC2134_ha2). Since we had noticed these two distinct points of Hα emission in the AGC2134 image we thought that perhaps there are more isolated points of Hα in the same image. So we did a thorough visual search of the AGC2134 Hα continuum-subtracted image. We did not find any more Hα dots by carefully searching the image by eye. However, the Hα dot software found not only the two Hα dots that had initially been found by eye, but it also found an additional Hα dot in the image that had been missed by the thorough visual search. This example points out the power of the software. The software is very sensitive to faint objects and allows us to find not only isolated regions of Hα that are obvious in the image but also much fainter dots of Hα emission that would be missed by just a visual inspection. Of course, visually inspecting each potential Hα dot candidate selected by the software is critical to verifying that the object appears to be real when developing the Hα dot candidate list. Both the automatic software and careful visual inspection of each Hα dot candidate are integral to developing a complete sample of Hα dot candidates.

It is important to acknowledge that despite our best attempts to be complete

and objective when selecting the Hα dot candidates there is still room for improvement. The selection criteria based on the magnitude difference and ratio value has been rigorously defined. During the visual inspection of the Hα dot candidates, one of the criteria for an object to be considered an Hα dot candidate and not an HII region that is part of a larger galaxy is the compactness of the object. We have been consistent in visually imposing the criterion of compactness, and objects that are clearly extended have been re-classified as HII regions. However, this selection criterion of compactness could be more rigorous by considering the radial light profile of the object.

The Hα dot candidate catalogue in Table 5.1 represents a complete list of Hα dot candidates from all ALFALFA Hα images taken to date. Once more narrowband images are taken, they can be searched for more Hα dot candidates and the Hα dot candidate catalogue can be expanded.

5.2 Spectral Results

Once we had selected a sample of Hα dot candidates, we obtained follow-up spectra in order to uncover their nature and measure some of their physical properties. We took spectra of 29 Hα dot candidates in November 2007 at MDM. Ten of the 29 Hα dot candidates are not emission-line sources. Eight are background, high redshift emission-line objects and eleven are low redshift emission-line objects. We measured the relative strengths of the emission lines in order to distinguish star-forming regions from AGN as described in Chapter 4. All eleven of the low redshift Hα dots are star-forming regions. Of the eight high redshift objects, two are probably Seyfert 2 galaxies, one is a quasar, and for five of them, the type can not be determined given the current data. Once we take more data toward the red

end of the spectrum of these high redshift Hα dots, we will be able to definetively classify them as star-forming regions or AGN. In Chapter 4, the physical properties of the Hα dots are presented. Emission-line ratios - including [O III]/Hβ and [N II]/Hα - are presented in Table 4.1. In addition the redshift is measured for each Hα dot and the velocity is calculated for the low redshift Hα dot sample. We also compute abundance estimates for the low redshift Hα dot sample. In addition to taking spectra of 29 Hα dot candidates in November 2007, we also took spectra of 32 Hα dot candidates in March 2008. From the March spectra, six of the Hα dot candidates are not emission-line sources. Sixteen are low redshift emission-line sources and 10 are high redshift emission-line sources. Currently, we are still in the process of reducing the spectra taken in March. Once we finish reducing the spectra we can analyze this sample as was done for the November spectra.

5.3 Surface and Volume Density of Hα Dots

Now that we have selected our sample of Hα dots, we can calculate some of their global properties. Two interesting quantities to calculate are the surface density and volume density of the Hα dots. The Hα dot script was run on 205 fields. Two 20 minute integrations were obtained of each field. For four of the fields, one of the Hα images was not usable because of heavy cloud cover. In order to be consistent, these four fields (and the one Hα dot - AGC223205_hadot1 - that was found in one of these fields) are excluded from the surface and volume density calculations. Also, the six false detections are excluded from the calculation. We will assume that the 11 Hα dot candidates from the fall that have not yet been spectroscopically confirmed are all real emission-line sources. Taking into account

the above considerations, our survey includes 201 fields and has detected 53 Hα dots.

The size of the field for the March 2006, May 2007, September 2006, and October 2007 datasets (176 fields) is 15 x 15 arcminutes. The size of the field for February 2007 (25) is 10 x 10 arcminutes. So the total area covered by the Hα dot survey is 42,100 square arcmin or 11.694 square degrees. The surface density is calculated according to the following equation:

$$Surface\ Density = \frac{Number\ of\ H\alpha\ dots}{Area\ of\ Sky\ Covered\ by\ Survey}. \tag{5.1}$$

The surface density of the Hα dot survey is 4.53 Hα dots per square degree.

In order to gain insight into the depth and sensitivity of the Hα dot survey, it is interesting to compare the surface density of the Hα dot survey to the surface density of other emission-lines survey. The overall surface density of the KISS emission-line galaxies is 16.84 per square degree. However, since it is an objective-prism survey, the KISS survey covers a much larger redshift range than the Hα dot survey. For the KISS galaxies in the redshift range covered by the Hα dots (1460 - 7810 km/s, which corresponds to the narrowband filters HA2-HA4) the surface density is 1.34 per square degree (Salzer, private communication). This is only 30 percent of the Hα dot surface density. So the KISS survey has the benefit of covering a much larger range in redshift, while the Hα dot survey has the benefit of going deeper within a more restricted redshift range.

In addition to calculating the surface density of the Hα dots, we also calculated the volume density of the low redshift Hα dots. In order to calculate the volume density of the Hα dots we need to compute the volume included in the Hα dot survey. The narrowband images were taken in four different Hα filters each

Table 5.2: Hα Filters

Filter	Velocity$_1$ (km/s)	Velocity$_2$ (km/s)	Width (A)
HA1	0	1460	67
HA2	1460	3150	74
HA3	3150	5300	68
HA4	5300	7810	71

covering a different velocity range. The velocity range covered by each of the four filters - HA1, HA2, HA3, and HA4 - is shown in Table 5.2.

The total volume covered by each filter was calculated by multiplying the percent area covered by the filter times the volume of the spherical annulus for each filter. The percent area covered by each filter was calculated by dividing the area covered by each filter by the total area of the sky (41,253 square degrees). The volume of the spherical annulus for each filter was calculated according to the following formula:

$$Volume\ (Spherical\ Annulus) = \frac{4}{3}\pi D_2^3 - \frac{4}{3}\pi D_1^3. \tag{5.2}$$

D_1 and D_2 represent the inner and outer distances of the spherical annulus. D_1 and D_2 are calculated from Velocity$_1$ and Velocity$_2$ for each filter from Table 5.2. The conversion from velocity to distance is made using Hubble's law.

$$v = H_o D. \tag{5.3}$$

Once we had calculated the volume included in each of the four filters we added the volumes together to calculate the total volume covered by the survey. The total volume covered by the survey is 433.3 Mpc^3. Next we determined the number of low redshift Hα dots in the Hα dot sample. 27 of the 46 real spectroscopically

confirmed emission-line objects are low redshift. Based on this, we assume that 59 percent of the 11 Hα dot candidates that have not yet been observed spectroscopically are low redshift. Adding together the 27 spectroscopically confirmed low redshift Hα dots and the 6 assumed low redshift Hα dots, we have a total of 33 low redshift Hα dots detected in the Hα dot survey. The volume density of the low redshift Hα dots is computed according to the following equation:

$$Volume\ Density\ (low\ z) = \frac{Number\ of\ low\ z\ H\alpha\ dots}{Volume\ Covered\ by\ Survey}. \tag{5.4}$$

The volume density of the low redshift Hα dots is 0.0762(low z Hα dots)/Mpc^3.

5.4 Projected Distance Between Hα Dot and Galaxy

For the low redshift Hα dot sample, the angular separation and projected distance between the Hα dot and the nearest galaxy have been calculated. The proximity of the Hα dot to the nearest galaxy is an interesting quantity to compute because it will help us distinguish between isolated extragalactic HII regions and dwarf galaxies. Typically extragalactic HII regions will be closer to the nearest galaxy than dwarf galaxies. In order to definetively distinguish between HII regions and dwarf galaxies it would be necessary to take HI observations in order to determine if the Hα dot is connected to the nearest galaxy by a tidal stream. However, measuring the projected distance between the Hα dot and the nearest galaxy will give an idea of the environment around the Hα dot.

In order to measure the projected distance, we displayed the field that contained the Hα dot candidate and identified the nearest galaxy. The x and y pixel positions of the Hα dot and nearest galaxy are recorded. The separation in pixels

is calculated using the pythagorean theorem. The angular separation in arcseconds is calculated by multiplying the separation in pixels by the image scale of 0.6 arcsec per pixel. Using the velocity of the target galaxy from the ALFALFA website, we calculate the distance to the galaxy and Hα dot using Hubble's law. Next we calculate the projected distance between the Hα dot and the galaxy according to the following formula:

$$Projected\ Distance = Distance\ x\ Sin(angular\ separation) \tag{5.5}$$

When doing these calculations we assume that the low redshift Hα dot is at the same redshift as the galaxy. This is not necessarily true, but for the low redshift Hα dot sample, this is a good approximation.

Presented in the table below are the angular separations and projected distances between the Hα dot and the nearest galaxy.

5.5 Star Formation Rate

The star formation rate for the low redshift Hα dot sample has been calculated. Photometry was done on each Hα dot in the Hα continuum-subtracted image. A photometry script (Sugden 2008) that incorporates the IRAF task `phot` was used to measure the magnitude and associated error. When doing photometry it is important to choose the correct aperature size to use. For measuring total magnitudes it is important to choose an aperature size that includes all the light from the object. Since we are trying to measure total magnitudes, the aperature size was chosen to include all the light from the Hα dot. The size of the aperature that was used varied from Hα dot to Hα dot but was typically small (radius of 3-4

Table 5.3: Projected Distance

Name	Angular Separation (arcsec)	Velocity (km/s)	Distance (Mpc)	Projected Distance (Kpc)
(1)	(2)	(3)	(4)	(5)
agc002134_ha2	189	4586	61	56
agc102270_ha2	231	5232	69	78
agc100381_ha2	547	5171	68	182
agc101822_ha3	414	5129	68	137
agc101827_ha1	493	4935	65	157
agc120207_ha2	251	-	-	-
agc332915_ha2	417	3564	47	96
agc332921_ha1	359	3650	48	84
agc438_ha2	371	-	-	-
agc007817_ha1	135	2737	36	23
agc182483_ha1	5	3302	44	1
agc182483_ha2	34	3302	44	7
agc182483_ha3	5	3302	44	1
agc215158_ha1	146	3201	42	30
agc220292_ha1	341	4992	66	110
agc223205_ha1	203	1787	23	23
agc8114_ha1	422	1990	26	54
agc009330_ha1	308	5128	68	102
agc010384_ha1	181	4967	66	58
agc010384_ha4	187	4967	66	60
agc010384_ha5	279	4967	66	89
agc230859_ha1	76	4497	59	22
agc242319_ha1	223	5245	69	75
agc242319_ha2	516	5245	69	174
agc262397_ha1	60	4954	66	19

arcseconds is common). Since the morphology of the Hα dots are compact and there is little diffuse light surrounding them, it is most appropriate to use a small aperature. The other important parameter to select is the width of the annulus from which the background level is calculated. An annulus width of 10 pixels was used. In the case that there were objects within the background annulus, these objects were masked out when doing the photometry. The instrumental magnitudes and their associated errors from `phot` were then converted to calibrated apparent magnitude. The method of calibration and conversion is described in Sugden 2008.

The Hα fluxes presented in the table still require several important corrections that have not yet been taken into account - [N II] correction, galactic absorption correction, and galaxian absorption correction. The [N II] correction is necessary because the width of the narrowband Hα filter is larger than just the Hα emission line. The narrowband Hα filter is about 65 to 70 Å wide. The rest wavelength of Hα is 6563 Å and the rest wavelength of [N II] is 6548 Å. Since these two emission lines are so close to each other, they are both detected by the Hα filter. Therefore the measured Hα flux must be corrected by removing the contribution from the [N II] emission line. The other two corrections - galactic absorption and galaxian absorption - account for absorption by dust. The galactic absorption correction accounts for absorption by dust within our galaxy. The galaxian absorption correction accounts for absorption by dust within the Hα dot host galaxy. Since none of these corrections have been taken into account yet, Hα fluxes, Hα luminosities, and star formation rates are approximate values. In the future, once we take more calibration images, we can take these corrections into account and present more accurate results. However, all of the corrections referred to above are expected to be small for our low luminosity Hα dot sample. Therefore we expect that the

luminosities and star formation rates presented below will be close to their final values.

The distance to the Hα dot was calculated using Hubble's law. The velocity of each Hα dot was determined from the spectral observations as described in Chapter 4. A Hubble constant of 75 km/s/Mpc was used when calculating the distance. Then based on the distance and the Hα flux from Table 5.4 the Hα luminosity is calculated using the following formula:

$$L = F4\pi D^2. \tag{5.6}$$

The luminosity of each low redshift Hα dot (in erg/s) is presented in Table 5.4.

Using the Hα luminosities, the star formation rate is calculated according to the following equation from Kennicutt 1998:

$$SFR(M_{sun}/year) = 7.9x10^{-42}L(H\alpha). \tag{5.7}$$

It is interesting to notice that some of the Hα fluxes of the Hα dots are very low. For example, the flux of AGC200496_5 is 7.1 x 10^{-16} erg/s/cm^2. The ability of the survey to detect objects with such low flux values suggests that the survey is very sensitive. Histograms of the fluxes of the Hα dots and ALFALFA galaxies (Sugden 2008) are presented in Figure 5.1. The median log(flux) value of the Hα dots is -14.63 erg/s/cm^2 and the median log(flux) value of the ALFALFA galaxies is -13.35 erg/s/cm^2. The Hα dots extend to much fainter flux limits than the ALFALFA galaxies.

Table 5.4: Hα dot Star Formation Rates

Name	diameter (arcsec)	f(Hα) (x10^{-14}) ($erg/s/cm^2$)	$\sigma_{f(H\alpha)}$ (x10^{-14}) ($erg/s/cm^2$)	L(Hα) (x10^{38}) (erg/s)	SFR ($M_\odot$/year)
(1)	(2)	(3)	(4)	(5)	(6)
AGC006666_1	10.0	0.198	0.042	-	-
AGC006653_1	8.0	0.075	0.017	-	-
AGC010176_1	8.0	0.305	0.023	-	-
AGC010384_1	6.0	0.230	0.019	12.063	0.00953
AGC010384_2	6.0	0.301	0.021	-	-
AGC010384_4	6.0	0.149	0.019	7.815	0.00617
AGC010384_5	8.0	3.681	0.056	193.073	0.152
AGC010384_6	6.0	0.176	0.021	-	-
AGC262397_1	10.0	0.477	0.022	24.888	0.0196
AGC009330_1	8.0	0.851	0.034	47.576	0.0376
AGC242319_1	8.0	0.191	0.038	11.171	0.00883
AGC242319_2	8.0	0.302	0.035	17.663	0.0139
AGC260281_1	6.0	0.333	0.016	-	-
AGC230859_1	10.0	0.990	0.037	42.564	0.0336
AGC100381_2	8.0	0.322	0.046	18.185	0.0143
AGC110790_1	6.0	0.097	0.020	-	-
AGC110790_5	6.0	0.082	0.020	-	-
AGC002026_2	20.0	6.769	0.118	-	-
AGC332915_2	8.0	0.412	0.028	34.161	0.0270
AGC122211_1	6.0	0.064	0.017	-	-
AGC101827_1	8.0	1.625	0.035	164.101	0.129
AGC332921_1	10.0	0.486	0.030	53.414	0.0422
AGC101822_1	8.0	0.136	0.029	-	-
AGC101822_3	10.0	0.515	0.043	56.444	0.0446
AGC101826_1	6.0	0.056	0.015	-	-
AGC001250_1	6.0	0.127	0.021	-	-
AGC001955_1	6.0	0.136	0.025	-	-
AGC100489_1	10.0	0.117	0.029	-	-
AGC331266_1	6.0	0.086	0.018	-	-
AGC000573_2	6.0	0.065	0.016	-	-
AGC120207_1	6.0	0.174	0.023	-	-
AGC120207_2	6.0	0.147	0.023	9.402	0.00743
AGC000438_1	6.0	0.043	0.014	-	-
AGC000438_2	8.0	0.587	0.035	32.791	0.0259
AGC111945_1	6.0	0.135	0.029	-	-

Continued on next page

Table 5.4 – continued from previous page

Name	diameter (arcsec)	f(Hα) (x10^{-14}) ($erg/s/cm^2$)	σ (x10^{-14}) ($erg/s/cm^2$)	L(Hα) (x10^{38}) (erg/s)	SFR ($M_\odot$/year)
(1)	(2)	(3)	(4)	(5)	(6)
AGC332912_2	6.0	0.340	0.030	-	-
AGC001292_1	8.0	0.327	0.039	-	-
AGC002134_1	8.0	0.631	0.042	-	-
AGC002134_2	10.0	1.232	0.051	50.893	0.0402
AGC002134_3	8.0	0.090	0.034	-	-
AGC122418_1	8.0	0.151	0.038	-	-
AGC102270_2	6.0	0.413	0.031	23.505	0.0185
AGC102268_2	6.0	0.148	0.025	-	-
AGC215158_1	10.0	0.324	0.042	8.725	0.00689
AGC220292_1	10.0	0.413	0.043	21.881	0.0172
AGC182483_1	10.0	0.553	0.028	12.818	0.0101
AGC182483_2	10.0	1.186	0.032	27.492	0.0217
AGC182483_3	8.0	0.613	0.024	14.209	0.0112
AGC200496_1	8.0	0.091	0.024	-	-
AGC200496_5	6.0	0.071	0.018	-	-
AGC200496_7	6.0	0.128	0.019	-	-
AGC223205_1	8.0	0.810	0.058	5.505	0.00435
AGC008114_1	8.0	0.378	0.039	3.182	0.00251
AGC007817_1	8.0	0.211	0.033	3.367	0.00266
AGC211006_1	6.0	0.166	0.015	-	-
AGC200598_4	8.0	0.237	0.046	-	-

5.6 Nature of Hα Dots

One of the goals of this thesis is to understand the nature of Hα dots. When this thesis began with the unexpected discovery of two small point sources in a single image we had no idea what Hα dots were or whether or not more than two of them existed. By writing software to search for them in over 200 images and taking follow-up spectra of about 60 Hα dot candidates we have now begun to

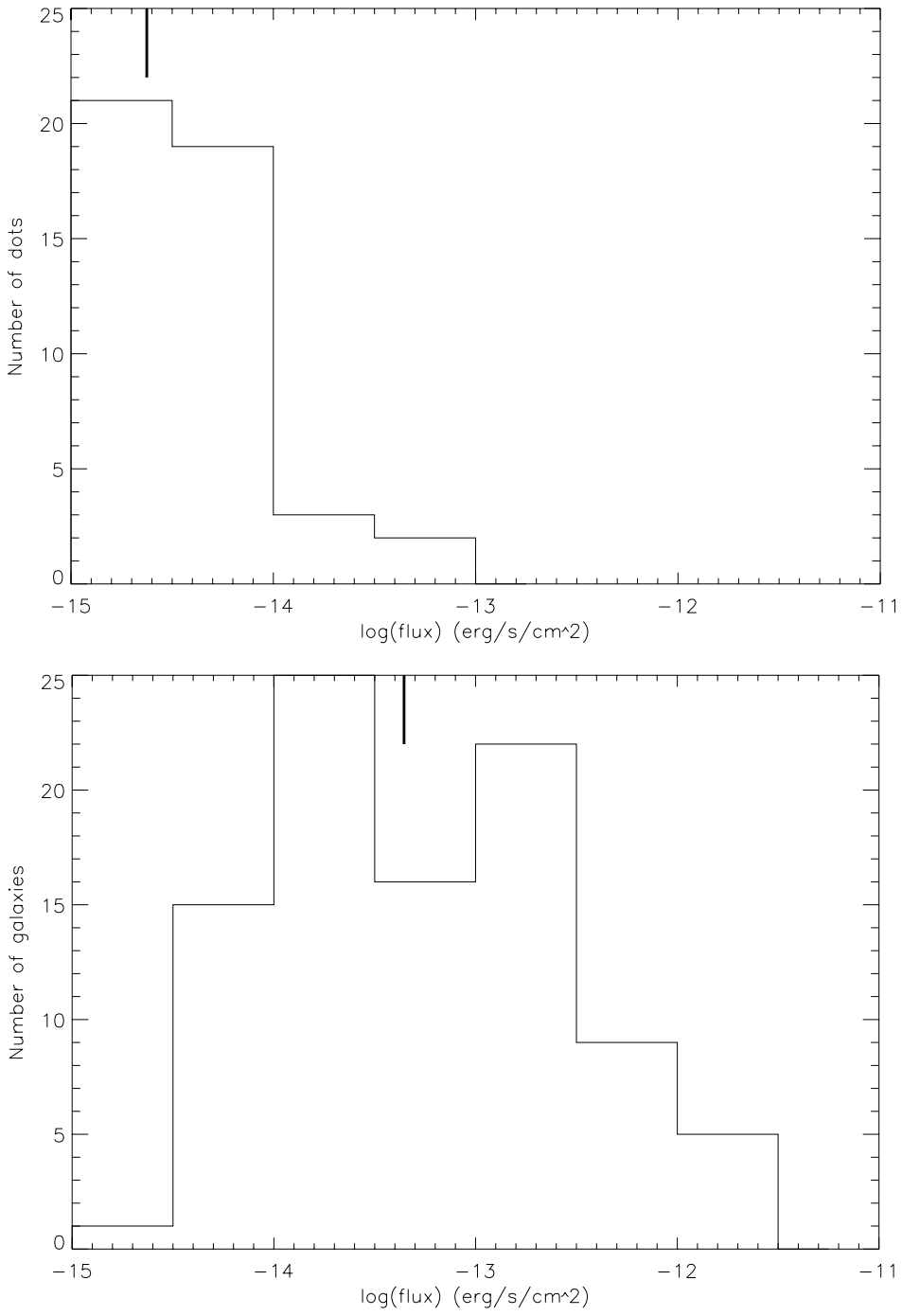

Figure 5.1: Histograms of the fluxes of the Hα dots (upper histogram) and ALFALFA galaxies (lower histogram), respectively. The vertical mark at the top of each graph reflects the median value.

uncover their nature. We know that they are a combination of two different types of emission-line sources: AGN and star-forming regions. Some of the AGN are Seyfert II galaxies and a couple are quasars. Some of the star-forming regions are low-luminosity dwarf galaxies and some of the star-forming regions may be isolated extragalactic HII regions. In order to determine if any of them are extragalactic HII regions, it would be necessary to take HI observations. The Hα dots are at a variety of redshifts. Some are background high redshift objects and some are low redshift objects at the same redshift as the ALFALFA target galaxy. We have also gained insight into the chemical composition of the Hα dots by measuring their abundances. They tend to be metal poor, and in particular, two of the Hα dots are extremely metal poor. The software and selection techniques that have been developed specifically for this survey are sensitive to very faint flux levels. Many of the low redshift Hα dots have very low Hα luminosities and low star-formation rates. We have calculated the surface density and volume density of the Hα dots to give us an idea of how common they are in the universe. Throughout this thesis, we have learned a great deal about the nature of Hα dots.

Perhaps more intriguing than what we now know about Hα dots, is what we do not yet know. We still lack a complete understanding of the environment around the Hα dots. Are they connected to nearby larger galaxies or are they independent objects? Also, the formation of the Hα dots still remains a mystery. Did the Hα dots just begin forming stars recently or have they been forming stars for a long time but are unable to retain their metals? And finally, we have yet to fully address one of the most fundamental questions of the entire thesis. What causes star formation to occur in the space between the galaxies?

Chapter 6

Conclusion and Future Work

6.1 Answering the Questions

This thesis is a "spin-off" project. The data that were used to do the Hα dot project were not originally taken for this purpose. The Hα narrow-band images in which the Hα dots were found were taken as part of a much larger project to calculate the star formation rate in the local universe (Sugden 2008). The discovery of the Hα dots was unexpected and since they seemed intriguing, we sought to understand as much about them as possible. When we began the project we did not know whether more than two Hα dots existed and whether they were even real emission-line sources. Initially when we noticed the two isolated dots in the data, we assumed that a mistake had been made in the image reduction process and that the dots were some type of detector artifact rather than representative of true objects in the universe. It was not until we took our first set of follow-up spectra in November 2007, that we could definitively confirm that the Hα dots are in fact real emission-line sources.

One of the main focuses of this thesis is the development and design of the Hα

dot survey. In order to fully study and understand a class of objects it is necessary that the selection method and criteria are well thought-out and tested and that the candidate objects are selected in a rigorous and consistent manner. When designing a survey there are many options in terms of how to detect objects and many choices to be made about how to select them. Therefore, much emphasis was placed on finding our Hα dot candidates in the most rigorous and complete way possible. Our ability to say anything meaningful about these objects depends critically on the way in which we select them. One of the successes of the Hα dot survey is its ability to extend to very low flux limits. Although the survey began with the discovery by eye of two Hα dots in a single image, we have now detected many Hα dots that would never have been noticed visually.

The spectra not only reveal that the Hα dots are real, but they also provide us with insight into their nature and give us a great deal of information about their physical properties. We now know that the Hα dots are a combination of AGN and star-forming regions. Some of the AGN are Seyfert 2 galaxies and some are quasars at redshifts as high as z=3.3. The star-forming regions are particularly interesting because of their low luminosity and low metallicity. They represent instances of extremely isolated and small occurances of star formation within our universe. Typically star formation occurs in larger galaxies, so it is interesting to study the unusual instances of star formation occuring in isolation. Not many stars are being formed in these Hα dots as shown by their very low star formation rates. The fact that star formation would occur at all in these small isolated regions between larger galaxies is intriguing.

6.2 Questioning the Answers

We would like to emphasize that this thesis does not represent a completed project. It is simply an honest and thorough description of the questions that have been asked, the analysis that has been done, and the ideas that have been conceived of to date. There is no doubt that given more time the project can and will continue to evolve naturally.

One question that has not yet been fully addressed is whether the star forming Hα dots are isolated extragalactic HII regions or dwarf galaxies. In order to answer this question, it is necessary to gain insight into the environment around the Hα dots. Are they connected to nearby galaxies by tidal streams or are they truly instances of isolated star formation events? One way to answer this question would be to take HI VLA observations of the Hα dots. By studying the surrounding neutral hydrogen in detail, we can determine in what way they are related to the galaxies around them. We are planning to write a VLA proposal to do this.

This thesis has focused entirely on studying objects based on the light we can observe. We have detected and studied the Hα dots through the photons they emit from either star formation processes or accretion onto a black hole. A significant amount of the universe does not emit light that is detectable in the electromagnetic spectrum. About 25 percent of the universe is composed of dark matter. We can only infer the existence of dark matter through the effects it has on objects which we can observe. Do the Hα dots contain dark matter and if so how much? We may be able to answer this question by comparing the dynamical mass of the Hα dots to their luminous mass. The dynamical mass can be obtained by taking HI VLA observations and analyzing the rotation curves of the objects. The luminous mass can be obtained by taking observations in the near infared

since that part of the electromagnetic spectrum is relatively free of obscuration by dust. If the dynamical mass is much larger than the luminous mass, we can infer the existance of dark matter.

Another pressing question is what caused star formation to begin in these Hα dots in the first place, and for how long have they been forming stars. The chemical abundances give us a hint at answering this question. The Hα dots are very low metallicity. Their low metallicity could be explained in two different ways. We know that the Hα dots are low luminosity and that low luminosity objects tend to have low masses. Therefore perhaps the Hα dots are not able to retain the metals that are produced by supernova explosions. In this case they may have been forming stars for a long time but are unable to retain their metals because of their low escape velocity. The other option is that the Hα dots are low metallicity because they have just recently begun forming stars. Perhaps two hydrogen gas clouds just collided and it just became dense enough for star formation to begin. It is difficult to distinguish between these two possibilities observationally. One way to determine if the Hα dots have been unable to retain their metals is to study the intergalactic medium surrounding the Hα dots. By studying the absorption lines of quasars, the abundance of the intergalactic medium can be determined (Kilgard, private communication). This is difficult to do observationally because it would require the unlikely coincidence that a very bright quasar is near an Hα dot on the sky.

We would like to gain more insight into these unusual instances of star formation in the Hα dots by looking for UV halos. We would like to determine if the Hα dots are in the UV halos of the original target galaxies (Kilgard, private communication). We are planning to write a GALAX proposal to do this.

Another interesting avenue to pursue is to study the high redshift star-forming

Hα dots in more depth. By taking more spectra of the high redshift Hα dots we will be able to distinguish star-forming regions from AGN for the high redshift sample and study the properties of star-forming galaxies at a redshift of about 0.32.

Two of the low redshift Hα dots are particularly interesting because of their extremely low abundances. We would like to take higher quality spectra of these extremely metal poor Hα dots in order to get more accurate abundances.

At the time of writing this thesis, the spectra of the Hα dots obtained at MDM in March 2008 has not yet been fully reduced and analyzed. These spectra will be reduced and analyzed as was done for the November 2007 spectra and we will be able to distinguish between AGN and star-forming regions, measure redshifts, and measure abundances. Also, we will derive more accurate abundances for the low redshift Hα dots using ELSA (Johnson 2007).

In addition, we have just recently obtained more narrow-band images from the 0.9 meter telescope at Kitt Peak. Once these data are fully reduced, they will be searched for more Hα dots.

We have listed many ideas in the above paragraphs ranging from the more practical to the slightly more "crazy". There is no doubt that as the answers to the questions mentioned above are persued more questions will continue to arise!

Bibliography

[] Barnes et al. 2001, 154, 531.

[] Boroson, Salzer, and Trotter 1993, The Astronomical Journal, 412, 524.

[] Carrol and Ostlie, An Introduction to Modern Astrophysics. Weber State University, 1996.

[] Dopita and Evans 1986, The Astronomical Journal, 310, 15.

[] Giovanelli, et al. 2005, The Astronomical Journal, 130, 261.

[] Griffiths, Introduction to Quantum Mechanics, Pearson Prentice Hall, 2005.

[] Johnson, 2007, Nebular Abundances in Star-Forming Dwarf Galaxies, BA thesis.

[] Kennicutt, et al. 1998, The Astronomical Journal, 36, 189.

[] Meyer et al. 2003, The Astronomical Journal, 68, 580.

[] Osterbrock, Astrophysics of Gaseous Nebulae and Active Galactic Nuclei, University Science Books, 1989.

[] Payne-Gaposchkin, 1925, Stellar Atmospheres, PhD thesis.

[] Ryan-Weber, et al. 2003, The Astronomical Journal, 127, 1431.

[] Salzer et al. 2005, The Astronomical Journal, 624, 661.

[] Salzer, J. J., et al. 2000, The Astronomical Journal, 120, 80.

[] Salzer 1989, The Astronomical Journal, 347, 152.

[] Sugden 2008, ALFALFA Hα: The Star-Formation-Rate Density of the Local Universe, BA thesis.

[] van Dokkum, P.G. 2001, PASP, 113, 1420.

[] Werk et al., in preparation.